CSIRO Marine Laboratories
Report 204

Design of an Ocean Temperature Observing Network in the Seas North of Australia

Part 1. Tropical Pacific Ocean: Statistics

Gary Meyers
Janet Sprintall
Helen Phillips
Jan Peterson
Tomas Fonseca

1989

National Library of Australia Cataloguing-in-Publication Entry

Design of an ocean temperature observing network in the seas north of Australia. Part 1, Tropical Pacific Ocean : statistics.

ISSN 0725-4598
ISBN 0 643 04832 4.

1. Ocean temperature - Pacific Ocean - Measurement.
2. Ocean temperature - Pacific Ocean - Statistics.
I. Meyers, Gary. II.CSIRO. Marine Laboratories. (Series : Report (CSIRO Marine Laboratories); no. 204).

551. 46'01'09164

Printed by Rank Xerox Australia Pty Ltd Melbourne ESS/PAS 4/89 600

Design of an Ocean Temperature Observing Network in the Seas North of Australia

Part 1. Tropical Pacific Ocean: Statistics

Gary Meyers[1]
Janet Sprintall[2]
Helen Phillips[1]
Jan Peterson[1]
Tomas Fonseca[3]

CSIRO Marine Laboratories Report 204

1 CSIRO Division of Oceanography, Hobart, Australia
2 University of Sydney, Sydney, Australia
3 Universidad Catolica, Valparaiso, Chile

Abstract

This report is a compilation of the statistical data required for design of an ocean temperature observing network in the tropical Pacific, using the method of optimum interpolation (OI). The statistics were estimated from a data base of expendable bathythermograph observations on the shipping routes New Caledonia–Japan; New Caledonia–Hawaii and Tahiti–Panama. The temporal and meridional autocorrelation function (ACF) for the sea-surface temperature and depth of the 20°C isotherm was estimated at each degree latitude on each route. Additional data were used to estimate the zonal ACF. The ACF statistics permit estimation of the parameters required for OI: levels of signal and noise variance for each field and spatial/temporal decorrelation scales. The OI parameters are then summarised in large areas selected to represent the major currents.

I. Introduction

A network for observing ocean temperature has been established under the auspices of the World Climate Research Program/Tropical Oceans and Global Atmosphere Program (WCRP, 1985). The objectives are: to document and describe thermal variability in sufficient detail to understand the processes that control it; and to obtain the thermal data required to initialise dynamical models for prediction of climate. Ideally, the network should resolve thermal variability in the open ocean, with spatial scales larger than 100 km (meridional) by 1000 km (zonal), and time scales greater than one month. Smaller resolution is required in some boundary regions (such as the western boundaries, the equator and passages of Indonesian throughflow). The Implementation Plan prepared by the international TOGA Project Office (ITPO, 1987) requires an accuracy 0.25°C for temperature measurements at these scales. This report is the first of a series that will assemble the statistical information required to design and optimise sampling in the area that has the greatest control over Australian climate.

Plans for the TOGA ocean temperature observing network (ITPO, 1987) called for three methods of thermal data collection: (1) expendable bathythermograph (XBT) by ships-of-opportunity; (2) fixed temperature moorings with sensors in the upper 200 m – 500 m; and (3) satellite-tracked drifting buoys, with sensors either in the upper 200 m or at the surface only. The first step was to make maximum use of ships-of-opportunity (i.e. voluntary observing ships from the Merchant Marine), because this is the most cost effective method of obtaining coverage of large areas. The goal was to use enough ships to obtain 18–24 transects per year on as many transequatorial routes as possible. Oceanographic experience since the 1950s (Wyrtki et al., 1977) indicates that XBT stations should be spaced approximately 1° latitude apart, which required observations every 4–6 hours. The second step was to deploy temperature moorings wherever continuous time-series might be required, such as near the equator. Finally, drifting buoys would be deployed where prevailing currents would carry them into areas between ship-of-opportunity tracks. Some progress has been made since 1985, when TOGA began, in deploying all three methods. The network now needs to be optimised by finding the right mix of temperature sampling methods that are both cost effective and accurate.

The standard method of determining a sampling strategy in oceanography is optimal interpolation (OI) (Gandin, 1963; Alaka and Elvander, 1972; Bretherton, Davis and Fandry, 1976; White and Bernstein, 1979; White, Meyers and Hasunuma, 1982). Before this method can be applied, certain statistics of the field of interest — in this case either temperature or isotherm depth — must be known or estimated. The required statistics are: (1) variance of the signal of interest, (2) variance of the instrumental noise (usually negligible), or more importantly geophysical noise (i.e. unresolved thermal variability with scales smaller than the typical distance between XBT drops), and (3) spatial and temporal autocorrelation function (ACF) of the field of interest. If not known from theory, these statistics have to be determined from a data set — preferably one that has considerably oversampled the signals of interest.

A prototype of the TOGA XBT-network has been in operation since 1979 (Donguy, 1980; Meyers and Donguy, 1980; Donguy and Henin, 1981; White et al., 1985; Donguy, 1987; Meyers et al., 1988). This network collected transects, usually between 20°N and 20°S, near the shipping routes: New Caledonia–Japan, New Caledonia–Hawaii and Tahiti–Panama. These relatively long time-series are a unique resource, which can be used to estimate the OI statistics. A particularly important aspect of the data set is that it includes the 1982/83 episode of El Nino Southern Oscillation (ENSO), which can be expected to greatly influence any of the statistics having to do with variability (Meyers, 1982).

The OI statistics estimated with this data set are reported here. The mean and standard deviation of properties along the three transects are presented in Section II. Estimates of the temporal/spatial ACF are presented in Section III. Decorrelation scales and signal-to-noise ratios are presented in Section IV. Drawing on additional data, estimates of the zonal ACF are presented in Section V. Finally, an attempt is made in Section VI to summarise and schematicise the statistical structure across the tropical Pacific.

The parameters selected for statistical analysis were temperature at 3.7 m depth, called "sea-surface temperature" (SST), vertically averaged temperature over 200 m and 400 m (called "T_{200}" and "T_{400}") and depth of the 25°C, 20°C and 15°C isotherms (called "D_{25}", "D_{20}" and "D_{15}"). This report presents a selection of the results, primarily as visual displays, and primarily for SST and D_{20}. Tabulated values of all the results were saved in computer compatible format; they can be provided to interested users upon request.

II. Mean and Standard Deviation

The mean and standard deviation of temperature on each track were calculated for two time periods: June 1979–May 1982 and June 1979–May 1983. The second period includes the 1982/83 ENSO, which causes a significant change in estimates of standard deviation. Mean values, in contrast, are not perceptibly different for the two periods. Illustrations are presented for the mean and standard deviation of both periods (Figures 1 to 3).

III. Autocorrelation Functions

A. Temporal Structure

The ACF for time-lags of 0.5 to 11.5 months and negligible average separation in space was estimated for each degree latitude on the three tracks. To show the difference between the ACF during 1982/83 and the ACF during years with a more common level of interannual variation, the estimate was made for two time periods: June 1979–May 1982, and June 1979–May 1983. The temporal ACFs are displayed in groups of three for each degree latitude for SST (Figures 4, 6 and 8) and

for D_{20} (Figures 5, 7, and 9) for the Japan, Hawaii and Panama tracks, respectively.

The method of estimating these ACFs had to take into account the random sampling pattern of XBTs by ships-of-opportunity. First, for each degree latitude on the three tracks, all the XBTs within ± 1° latitude were assembled into a separate file for that location. The all data average for each of the parameters of interest was used to calculate a residual value for each XBT drop. Spatial biases had to be removed because the ships-of-opportunity did not always sail to the same port (see data location maps in Donguy, 1987). This caused a separation in longitude in excess of 12° on a portion of the central track (north of 10°N) and eastern track (south of 10°S). In these areas the average and residual values for each XBT drop were determined separately for tracks more than 12° apart. Note that this procedure removed spatial trends associated with mean thermal structure, but not seasonal variation.

The ACF was calculated by pairing values for the appropriate lag in one-month bins. In estimating values in the first bin (0 to 1 month lag), values were never paired with themselves so that the correlation in this bin would not be artificially raised by duplicate sampling of the geophysical noise. This requirement meant that in practice pairs in the first bin were usually separated by at least two weeks or 60 nautical miles because of the ship-of-opportunity sampling pattern of, at most, two cruises per month with samples every four hours.

B. Meridional Structure

The meridional structure of ACFs is expected to be non-isotropic with respect to lags northward and southward. For example, D_{20} in the Countercurrent Trough near 10°N is expected to have a negative correlation with D_{20} at 5°N, and a positive correlation with D_{20} at 15°N (Wyrtki, 1978). Isotropy was not assumed in estimating the spatial ACFs so that such structure could emerge where appropriate.

The ACF for latitude lags ± 6° and negligible average separation in time was estimated for each degree of latitude on the three tracks. The estimate was made for two time periods, as discussed in sections II and IIIA. The ACFs for SST are displayed in Figures 10,12 and 14; and for D_{20} in Figures 11, 13, and 15 for the Japan, Hawaii and Panama tracks, respectively.

The method of calculating these ACFs was to correlate the time-series of residual values defined in section IIA for appropriate spatial lags and a time lag of ± 1 month. Thus the value in the first bin of the temporal ACFs is the appropriate value for the zero-lag position on the meridional ACFs. The spatial structure represented in Figures 10 to 15 is, strictly speaking, representative of distance along the shipping track. It is most representative of meridional structure because zonal scales (discussed later) are much larger than meridional scales.

IV. Signal-to-Noise Ratio and Decorrelation Scales

The statistics needed for OI can be derived from estimated ACFs presented in the previous section, after appropriate assumptions (Alaka and Elvander, 1972).

The signal-to-noise ratio (α^2) is calculated by extrapolating the estimated ACFs into the origin (Gandin, 1963, p.30). Given the estimated value at the origin, μ_0, the ratio is:

$$\alpha^2 = \frac{\mu_0}{1 - \mu_0}$$

The value of μ_0 for this study was assumed to be the value of the temporal ACF (Section IIIA; Figures 4 – 9) in the first bin. Estimates of α for SST on the three tracks are shown in Fig. 16, and for D_{20} in Fig. 17 (note that α, not α^2, is plotted).

The variance of instrumental and geophysical noise (N^2) can be estimated from α and the measured standard deviation σ of the parameter of interest:

$$N^2 = \frac{\sigma^2}{\alpha^2 + 1} = \sigma^2(1 - \mu_o)$$

The instrumental noise is usually small, for the temperature sensing methods used by the TOGA network, so that N^2 is primarily associated with geophysical noise, such as eddies (which have a small space-scale) or weather events (which have a small time-scale). The variance of large-scale temperature signals (S^2) is:

$$S^2 = \sigma^2 - N^2 = \sigma^2 \mu_0$$

The signals have scales larger than the bin sizes used in estimating the ACFs (i.e. 1 month and 1° latitude).

The meridional structure of ACFs can be represented as a decorrelation scale, which is the typical size of coherent large-scale features. The meridional decorrelation scale was defined to be the e-folding scale measured on the estimated ACFs (Section IIIB, Figures 10-15). The scale was measured on the northward and southward sides and tabulated. The smaller of the two is the more stringent constraint in designing the network and is therefore the one presented in this report. The meridional scales for SST are presented in Figure 18, and for D_{20} in Figure 19.

The temporal structure of ACFs can also be represented as a decorrelation scale. The temporal structure of ocean temperature variability is often found to be either oscillatory (i.e. second order autoregressive process) (Chatfield, 1975) or characterised by increasing amplitude with longer time scales (first-order process). The appropriate decorrelation scale for a second-order process is the first zero crossing of the ACF. For a first-order process it is the e-folding scale. The appropriate scale was measured on the temporal ACFs (Section IIIA, Figs. 4-9). In most cases the e-folding scale was used and the zero-crossing selected only in cases where the ACF clearly showed a seasonal signal. The temporal scales for SST are presented in Fig. 20 and for D_{20} in Fig. 21.

V. Zonal Scales

A consistent set of zonal transects across the tropical Pacific has never, to our knowledge, been collected, so that a consistent analysis of zonal scales, using the methods described in III B is not possible. The zonal scale is nevertheless extremely important. The Pacific is the widest ocean, and uncertainty in the zonal scale can easily affect the optimal sampling density by a factor of two or more in the number of observations required each month. We have therefore assembled as much information as possible on this important parameter.

The temporal and meridional scales estimated in section III changed markedly, depending on whether an ENSO episode occurred during the period covered by the observations, and the same can be expected for zonal scales. We consider first the case that includes ENSO. Contour maps of the correlation between dynamic height relative to 500 db, on a grid covering the whole width of the Pacific, and sea level at a tide station were prepared by Hickey (1975) for stations in the latitude band 10°N to 10°S. Assuming that observations of sea level and dynamic height are measurements of the same oceanic field, Hickey's data can be rearranged into a zonal ACF for the latitude bands 2°N–2°S using sea level from Christmas and Canton Is. (Fig.22) and 6°–10°N using Truk and Kwajalein Is. (Fig. 23). The zonal scale under ENSO conditions is seen to be about 40° longitude, or one third the width of the basin. This scale is representative of changes in topography of the thermocline. While a similar scale for SST variability is not available, the thermocline scale is likely to be smaller, and the limiting factor in network design.

The zonal ACF for non-ENSO periods was estimated for the western, central and eastern Pacific (Fig. 24) for a variety of parameters that are all representative of the depth of the thermocline. The western region was covered by the Japanese Far Sea Fisheries (JFSF) BT sampling during the period 1968–1972. The distribution of data was shown in a report by White and Wylie (1977, Figs 17 and 18). The ACF was estimated for temperature at 400 m in the latitude band 5°–17°N (White et al., 1982). The central region was covered by the Trade Wind Zone Oceanography Study, January 1964–March 1965 (Meyers, 1975). The ACF was estimated for depth of the 20°C isotherm in the latitude band 5°–15°N. The eastern region was covered by the Eastropac cruises, 1967–1968 (Tsuchiya, 1972). The ACF was estimated for dynamic height 0/500 db in the latitude band 4°–12°N.

Another zonal ACF representative of non-ENSO years was estimated from the Master Oceanographic Observations Data Set (MOODS) from FNOC, Monterey CA (McLain, personal communication) covering the period January 1979 to December 1982. The ACF was estimated for depth of the 24°C isotherm (D_{24}) and average temperature above that isotherm (T_{24}), an alias of SST, in five latitude bands (see legend to figure) spanning the region 12°N–12°S. The calculations were made by Prof. T. Fonseca of Valparaiso University during a visit to Scripps Institution of Oceanography in 1983. Since MOODS is a random array, estimating the ACF was based on a binning procedure (White et al., 1982) using 1° latitude, 5° longitude, 1 month bins. Although the last four months of this data set contain ENSO signals, the fully matured ENSO anomalies were eliminated by the December 1982 cut-off. Thus we think that the scales are representative of the preceding non-ENSO years.

The zonal ACFs for non-ENSO periods (Figs 24 & 25) suggest a scale of 15° longitude for variability in the thermocline. This scale is in good agreement with the scale estimated from a hydrodynamic model (Kubota and O'Brien, 1987), which also showed that the scale decreases with increasing latitude to a value of 5° longitude in the subtropics. The estimated scale (15° longitude) is probably not applicable in areas more than 15° latitude from the equator.

VI. Summary of Statistical Structure

The estimation of scales derived from a comprehensive data set, as in sections III and IV, reveals a rich statistical structure in the thermal fields of the tropical Pacific. Optimal network design, or objective mapping of the fields, would not ordinarily attempt to represent all the detail of these scales, some of which is simply due to sampling of random fields. Also, however, it is preferable, particularly in mapping, to allow the structure of the observations to dominate over the statistical structure built into the analysis routine. Thus we seek a simplification of the statistics that is homogeneous over large areas and still representative of real structure in the ocean. With this goal in mind, three summaries of the essential OI statistics (spatial and temporal decorrelation scales, signal-to-noise ratios (α) and standard deviation(σ)) were prepared, representing three levels of increasing simplification.

A. Averages in 3° Latitude Bands

The ACFs (Figs. 4–15) indicate little change within 3° latitude bands. We have therefore averaged over the 3° bands. This summary essentially documents all of the meaningful detail in the statistics we have estimated. Tables 1 and 2 present the averages for SST for two time periods, as discussed earlier, one including the other not including the ENSO episode. Tables 3 and 4 present averages for D_{20}. Note that in averaging the variance-related statistics (α, σ), RMS values were calculated. The averaged meridional scale is the shorter of the northward and southward values. Scales greater than 6° latitude were set equal to 6°.

	WEST				CENTRAL				EAST			
	λ (°lat.)	τ (mo.)	α	σ (°C)	λ (°lat.)	τ (mo.)	α	σ (°C)	λ (°lat.)	τ (mo.)	α	σ (°C)
18 °N	6.0	3.0	2.9	1.1	6.0	2.7	0.7	1.0				
15	6.0	3.4	2.3	0.9	6.0	2.5	0.7	0.9				
12	6.0	3.4	2.9	0.8	6.0	2.8	0.8	0.8				
9	5.7	3.3	1.6	0.6	5.2	2.8	0.9	0.7				
6	3.7	2.2	0.9	0.4	5.6	2.7	0.8	0.6	6.0	1.6	1.0	1.1
3	4.9	1.2	0.5	0.4	5.7	1.4	0.7	0.8	5.7	2.7	0.9	1.7
0	4.6	1.1	0.5	0.4	5.9	1.4	0.7	0.8	6.0	3.1	1.6	1.9
3	3.1	1.8	0.8	0.5	5.6	2.5	0.6	0.6	6.0	3.4	1.8	1.6
6	4.9	2.3	1.0	0.6	5.8	5.3	0.8	0.6	6.0	3.2	1.2	1.1
9	5.4	3.1	1.9	0.9	5.4	2.6	1.0	0.5	6.0	3.0	0.9	0.9
12	6.0	3.1	1.7	1.1	5.5	2.6	1.4	0.7	6.0	2.4	0.8	1.0
15	6.0	3.1	1.7	1.3	6.0	2.9	2.0	1.0	6.0	3.1	1.1	1.0
18 °S	6.0	3.0	1.6	1.5	6.0	2.9	1.7	1.4	6.0	2.6	1.7	1.0

Table 1: SST 6/79 – 5/82 NON-ENSO PERIOD: Averaged scales for optimum interpolation. Meridional decorrelation (λ); temporal decorrelation (τ); RMS signal-to-noise ratio (α); RMS standard deviation (σ); on New Caledonia–Japan (WEST), New Caledonia–Hawaii (CENTRAL), and Tahiti–Panama (EAST) XBT tracks

	WEST				CENTRAL				EAST			
	λ (°lat.)	τ (mo.)	α	σ (°C)	λ (°lat.)	τ (mo.)	α	σ (°C)	λ (°lat.)	τ (mo.)	α	σ (°C)
18 °N	6.0	3.1	3.0	1.2	6.0	3.6	1.1	1.2				
15	6.0	3.2	3.1	1.1	6.0	3.6	1.2	1.1				
12	6.0	3.4	3.4	1.0	6.0	3.8	1.4	1.0				
9	6.0	2.8	2.1	0.8	5.2	2.6	1.3	0.8				
6	6.0	2.8	1.7	0.7	5.0	3.2	0.9	0.6	6.0	3.7	1.6	1.2
3	6.0	7.2	1.7	0.7	4.8	3.0	1.0	0.8	6.0	3.9	1.3	1.8
0	6.0	7.2	1.4	0.6	5.3	4.9	1.1	0.9	6.0	4.6	2.4	2.4
3	5.4	6.3	1.2	0.6	5.5	3.7	0.8	0.7	6.0	4.3	2.5	1.9
6	5.1	3.3	1.1	0.6	4.1	2.5	0.9	0.6	6.0	4.1	2.0	1.4
9	4.8	3.0	1.4	0.9	4.3	2.7	0.9	0.6	6.0	3.8	1.4	1.2
12	5.6	2.9	1.6	1.2	4.2	2.0	1.2	0.7	6.0	3.8	0.9	1.1
15	6.0	3.0	1.6	1.3	5.7	3.0	1.7	1.1	6.0	3.9	1.1	1.0
18 °S	6.0	3.0	1.6	1.5	6.0	3.1	1.6	1.4	6.0	2.6	1.4	1.0

Table 2: SST 6/79 – 5/83 ENSO: Averaged scales for optimum interpolation. As in Table 1.

	WEST				CENTRAL				EAST			
	λ (°lat.)	τ (mo.)	α	σ (°C)	λ (°lat.)	τ (mo)	α	σ (°C)	λ (°lat.)	τ (mo)	α	σ (°C)
18 °N	2.4	2.6	0.3	21	6.0	3.8	0.3	27				
15	2.7	2.3	0.5	15	4.6	2.4	0.8	25				
12	4.0	2.3	0.9	16	4.2	2.9	1.0	23				
9	3.2	2.8	1.1	13	2.5	3.9	0.9	19				
6	2.0	3.2	0.6	15	2.4	2.2	0.7	19	2.0	1.5	0.5	10
3	2.0	2.3	0.8	12	5.2	1.4	0.5	16	1.8	1.3	0.4	12
0	1.7	0.9	0.5	11	6.0	1.4	0.5	17	2.3	1.3	0.9	17
3	2.4	1.9	0.5	12	5.9	1.5	0.8	16	3.7	2.0	0.6	19
6	4.0	1.0	0.5	12	3.8	1.3	0.6	15	4.8	1.1	0.6	22
9	3.0	2.6	0.7	16	4.9	3.2	0.4	15	4.3	1.1	0.4	24
12	2.9	4.4	0.7	20	4.2	3.4	0.9	18	4.5	5.0	0.4	21
15	3.2	2.5	0.6	22	2.8	2.6	0.6	17	3.5	2.6	0.2	16
18 °S	3.4	2.7	0.4	29	2.1	1.2	0.5	29	3.4	2.4	0.5	19

Table 3. D_{20} 6/79 – 5/82 NON-ENSO PERIOD: Averaged scales for optimum interpolation. As in Table 1.

	WEST				CENTRAL				EAST			
	λ (°lat.)	τ (mo.)	α	σ (°C)	λ (°lat.)	τ (mo.)	α	σ (°C)	λ (°lat.)	τ (mo.)	α	σ (°C)
18 °N	4.6	1.6	0.4	21	6.0	4.0	0.3	26				
15	2.8	4.3	1.1	20	4.9	1.6	0.6	24				
12	5.2	3.8	1.9	23	4.7	3.2	1.0	23				
9	6.0	4.8	2.3	22	2.8	3.1	1.1	21				
6	6.0	3.7	1.5	20	2.7	1.8	0.8	19	6.0	5.6	1.7	17
3	6.0	4.5	1.4	18	3.6	2.8	0.9	19	6.0	6.4	1.9	24
0	6.0	4.7	1.2	16	5.8	3.5	1.2	22	6.0	5.4	2.5	30
3	6.0	4.8	1.3	18	6.0	4.3	1.4	22	6.0	3.1	1.4	25
6	5.2	5.5	1.7	20	6.0	4.1	1.9	28	5.9	2.9	0.9	22
9	3.3	4.1	1.2	19	5.8	4.2	2.6	30	5.4	1.1	0.5	23
12	3.8	3.0	0.7	19	4.5	3.7	1.8	22	4.6	5.2	0.4	21
15	3.7	2.3	0.6	21	5.1	2.4	0.7	18	3.6	2.6	0.3	16
18 °S	4.7	2.6	0.4	26	2.2	1.4	0.5	25	4.7	3.2	0.8	19

Table 4. D_{20} 6/79 – 5/83 ENSO: Averaged scales for optimum interpolation. As in Table 1.

B. Dynamic Subregions

The TOGA ocean temperature observing network will be designed to detect typical levels of interannual variability during the years between ENSO episodes. Tables 1 and 2 for non-ENSO periods were used to identify representative scales in geographical areas selected according to the baroclinic structure of the major zonal currents. The areas are shown in Figure 26. The equatorial wave-guide is the region 2°N to 2°S. The North Equatorial Countercurrent is the region 3°N to 12°N. The northern edge has been extended to 12°N to completely cover the Countercurrent trough, which has a baroclinic structure with very strong signal-to-noise ratios as far as 12°N (Table 3). The central North Equatorial Current is the region 12°N to 18°N. The South Equatorial Countercurrent is the region 3°S to 12°S, which also has high signal-to-noise ratios (Table 3) but not as high as the North Equatorial Counter Current. Finally the central South Equatorial Current is the region 12°S–18°S.

Space and time scales representative of the structure of the thermocline (Table 3) are smaller than the scales of SST, and more critical in designing the network. Representative scales for each region were chosen on the basis of, the strongest signals or frequently occurring values. The statistics for D_{20} are presented on a map in Fig. 27; and the rationale for their choice is presented below.

The strongest baroclinic signals are in the North Equatorial Coutercurrent, where a signal-to-noise ratio (α) of 1.0 appears in both the western and central Pacific (See Table 3). The RMS standard deviation σ is 15 m and 20 m, respectively. A meridional decorrelation scale of 3° latitude is representative of the estimates in Table 3. This scale appears because it is the half-width of the current. Baroclinic structures on either side of the NECC oscillate out of phase. A representative temporal decorrelation scale is 3 months because of the strong annual cycle in the North Equatorial Courtercurrent. The decorrelation scales are summarised in Fig. 28.

The signals in baroclinic structure in the equatorial wave guide are relatively weak. The signal-to-noise ratio α varies from 0.5 to 0.9. The values of σ are 12 m, 17 m and 17 m on the western, central and eastern tracks. A meridional decorrelation scale of 2° latitude is representative of the western and eastern tracks. A larger scale of 6° latitude appears in the central track, apparently because trapped Rossby waves have peaks of energy off the equator (Fig. 13A, bottom panels). A decorrelation time scale of 1.5 months is representative of all three tracks.

The South Equatorial Countercurrent has a moderately strong signal in the western and central tracks with $\alpha = 0.7$, and a weaker value in the east $\alpha = 0.5$. RMS values of σ are 13 m, 16 m, and 22 m. Meridional and temporal decorrelation scales of 4° latitude and three months are representative of all three tracks.

The scales for D_{20} in the North Equatorial Current and South Equatorial Current were estimated by averaging λ and τ, and root-mean-squared averaging α and σ from the values in Table 3. Scales for SST in all the areas were also determined by averaging and are displayed on the map in Fig. 28.

C. Uniform Scales

In some optimal mapping procedures it may be desirable to use one set of scales for the entire tropical Pacific, with the possible exclusion of boundary current regions. The experience gained in assembling the scales in this report leads to the following recommendations for mapping during non-ENSO periods. A meridional decorrelation scale of 3° latitude is consistent with most of the sub-regions of section VIB, particularly the North Equatorial Countercurrent. A zonal scale of 15° longitude is consistent with all the information from observations and models available at this time (see Section V). A time scale of two months is a compromise between the relatively rapid changes near the equator and the strong seasonal and longer period changes in the Countercurrents and SST fields (Fig. 28). The signal-to-noise ratio ranges from ~0.5 to >1 (Fig. 27). The recommended value is 1.0, which is representative of the North and South Countercurrents but is possibly an overestimate for the subsurface fields in other areas.

During ENSO, each of the scales is approximately doubled to 6° latitude (Tables 2, 4), 30° longitude (Section V), and 4 months (Tables 2, 4). The signal-to-noise ratio ranges from <1 to 2.5, with a typical value of 1.5.

References

Alaka, M.A. and R.C. Elvander, 1972: Optimum interpolation from observations of mixed quality. Man. Weath. Rev. **100**, 612-624.

Bretherton, F. P., R. E. Davis and C. B. Fandry, 1976: A technique for objective analysis and design of oceanographic experiments applied to MODE–73. Deep Sea Res. **23**, 559-582.

Chatfield, C., 1975: *The Analysis of Time-series*: Theory and Practice. Chapman and Hall, London, 263 pp.

Donguy, J.R., 1980: Rapport sur l'utilisation des navires non specialises. IOC WMO IGOSS-2 Doc. 5 Appendix A, Intergovernmental Oceanogr. Comm., Paris, 22 pp.

Donguy, J.R., 1987: Recent advances in the knowledge of the climatic variations in the tropical Pacific Ocean. 7. Oceanog. **19**, 49-85.

Donguy, J.R. and C. Henin, 1981: An expendable bathythermograph and sea surface temperature experiment in the eastern and western Pacific. Conference proceedings: Time series of Ocean Measurements, Tokyo 11-15 May 1981, World Climate Research Programme, 123-133.

Gandin, L. S. 1963: Objective analysis of Meteorological Fields, GIMI, Leningrad from Russian, Israel Program for Scientific Translations, Jerusalem, No. 1373. 242 pp.

Hickey, B. 1975: The relationship between fluctuations in sea level, wind stress and sea surface temperature in the equatorial Pacific. J. Phys. Oceanogr. **5**, 460–475.

ITPO, 1987: TOGA International Implementation Plan (Second Edition). International TOGA Project Office, World Meteorological Organisation, Geneva, 118 pp, 13 appendices.

Kubota, M., and J. J. O'Brien, 1988: Variability of the upper tropical Pacific Ocean Model. J. Geophys. Res. (submitted).

Meyers, G., 1975: Seasonal variation in transport of the Pacific North Equatorial Current relative to the wind field. J. Phys. Oceanogr. **5**, 442-449.

Meyers, G. and J.R. Donguy, 1980: An XBT network with Merchant ships. Trop. Ocean-Atmos. News. **2**, 6-7.

Meyers, G. 1982: Interannual variation in sea level near Truk Island — a bimodal seasonal cycle. J. Phys. Oceanogr. **12**, 1161–1168.

Meyers, G., J.R. Donguy, M. England, R. Reed, 1988: Heat storage in the tropical Pacific Ocean and the Southern Oscillation. Part I: Surface fluxes (Submitted for review).

Tsuchiya, M. 1972: A subsurface North Equatorial Countercurrent in the eastern Pacific Ocean. J. Geophys. Res. 77, 5981–5986.

WCRP, 1985: Scientific Plan for the Tropical Ocean and Global Atmosphere Programme, WCRP Publ. Ser. No. 3, World Meteorological Organisation, Geneva, 146pp.

White, W.B. and R.A. Wylie, 1977: Annual and seasonal maps of the residual temperature in the upper waters of the western north Pacific from 1954–1974, Scripps Institution of Oceanography Reference Series No. 77–28, La Jolla, 41 pp., 78 illustr.

White, W.B. and R.L. Bernstein, 1979: Design of an oceanographic network in the mid-latitude north Pacific. J. Phys. Oceanogr. **10**, 592–606.

White, W.B., G. Meyers and K. Hasunuma, 1982: Space/time statistics of short-term climatic variability in the western north Pacific. J. Geophys. Res., 87, 1979–89.

White, W.B., G. Meyers, J.R. Donguy and S.E. Pazan, 1985: Short term climatic variability in thermal structure of the Pacific Ocean during 1979–1982. J. Phys. Oceanogr. **15**, 917–935.

Wyrtki, K., G. Meyers, D. McLain and W. Patzent, 1977: Variability of the thermal structure in the central equatorial Pacific Ocean. Hawaii Inst. Geophys. Report HIG-77-1, 32pp.

Wyrtki, K., 1978: Monitoring the strength of equatorial currents from XBT sections and sea level. J. Geophys. Res. 83, 1935-40.

Illustrations

FIGURE 10A-E New Caledonia–Japan track. Sea surface temperature. Meridional autocorrelation function, in 3° latitude bands. The central latitude is indicated at the top of each frame, and its ACF indicated with dots. Lag is in degrees latitude; positive indicates northward separation.

FIGURE 11A-E New Caledonia–Japan track. Depth of 20°C isotherm. Meridional autocorrelation function. Details as in Fig. 10.

FIGURE 12A-E New Caledonia–Hawaii track. Sea surface temperature. Meridional autocorrelation function. Details as in Fig. 10.

FIGURE 13A-E New Caledonia–Hawaii track. Depth of 20°C isotherm. Meridional auto-correlation function. Details as in Fig. 10.

FIGURE 14A-C Tahiti –Panama track. Sea surface temperature. Meridional autocorrelation function. Details as in Fig. 10.

FIGURE 15A-C Tahiti–Panama track. Depth of 20°C isotherm. Meridional autocorrelation function. Details as in Fig. 10.

FIGURE 16A-C Signal to noise ratio of SST on the New Caledonia–Japan (A), New Caledonia–Hawaii (B) and Tahiti–Panama (C) tracks

FIGURE 17A-C Signal to noise ratio of D_{20} on three tracks as in Fig. 16.

FIGURE 18A-C Meridional decorrelation scale of SST on three tracks as in Fig. 16.

FIGURE 19A-C Meridional decorrelation scale of D_{20} on three tracks as in Fig. 16.

FIGURE 20A-C Temporal decorrelation scale of SST on three tracks as in Fig. 16.

FIGURE 21A-C Temporal decorrelation scale of D_{20} on three tracks as in Fig. 16.

FIGURE 22 Zonal autocorrelation function for dynamic height 0/500db, after Hickey (1975). 2°N–2°S, ENSO periods included.

FIGURE 23 Zonal autocorrelation function for dynamic height 0/500db, after Hickey (1975). 6°N–10°N, ENSO periods included.

FIGURE 24 Zonal autocorrelation function for various indices (see text) of the depth of the thermocline for non-ENSO periods.

FIGURE 25 Zonal autocorrelation function for the depth of the 24°C isotherm (D_{24}) and vertically averaged temperature between the surface and the isotherm (T_{24}), during June 1979 to November 1982.

FIGURE 26 Geographical areas where optimum interpolation statistics were summarised. North Equatorial Current (NEC); North Equatorial Countercurrent (NECC); Equatorial Wave Guide (EWG); South Equatorial Countercurrent (SECC); South Equatorial Current (SEC)

FIGURE 27 Signal-to-noise ratio (α) and standard deviation (σ) during non-ENSO periods. Values for sea surface temperature (SST) and depth of 20°C isotherm (D_{20}) as in legend.

FIGURE 28 Spatial and temporal decorrelation scales (λ , τ) during non-ENSO periods, as in Fig. 27.

Figure 1A

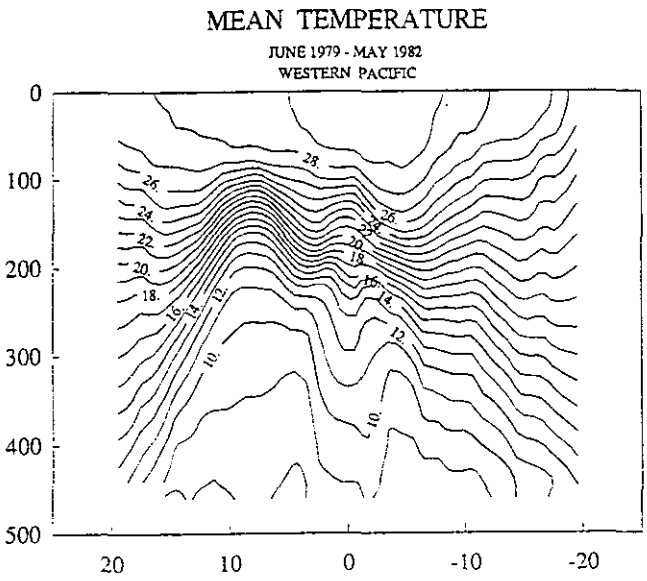

Figure 1B

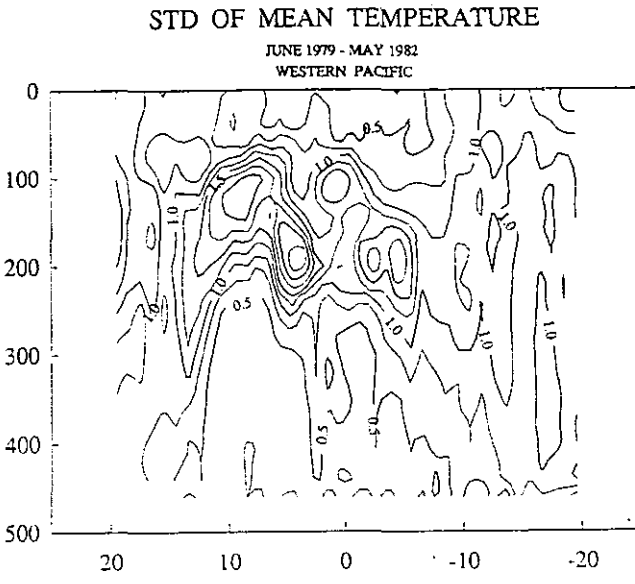

Figure 1C

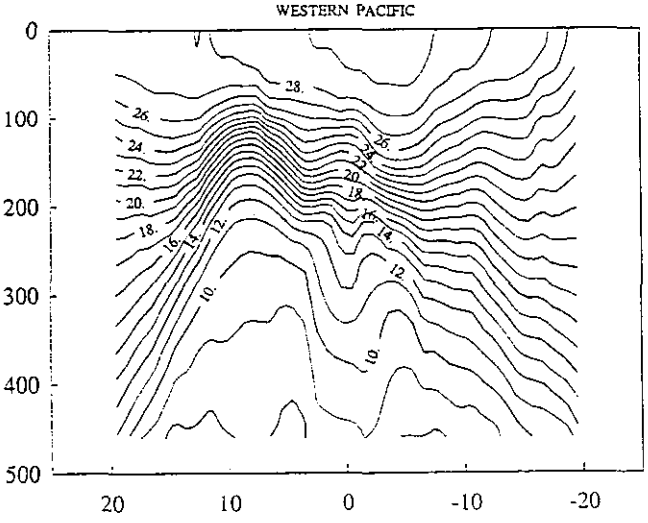

Figure 1D

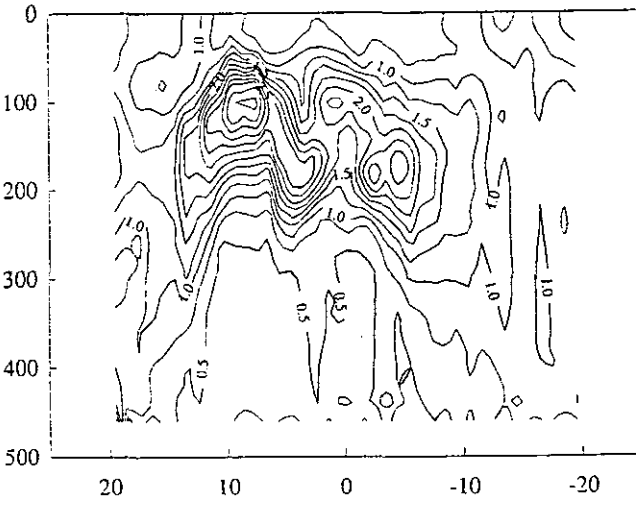

Figure 2A

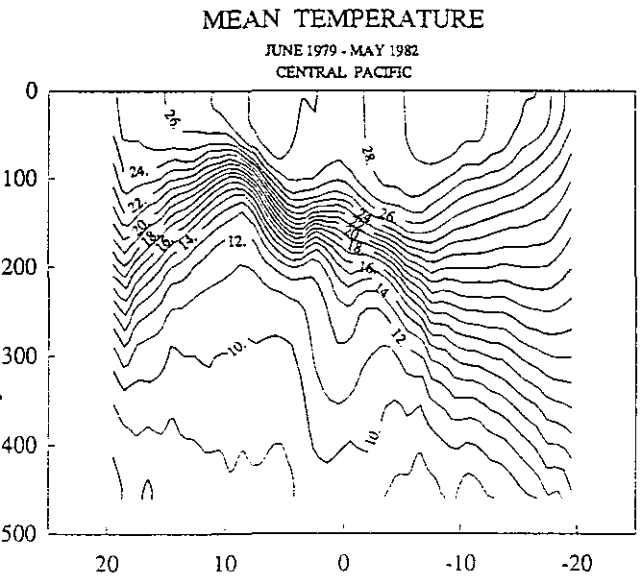

Figure 2B

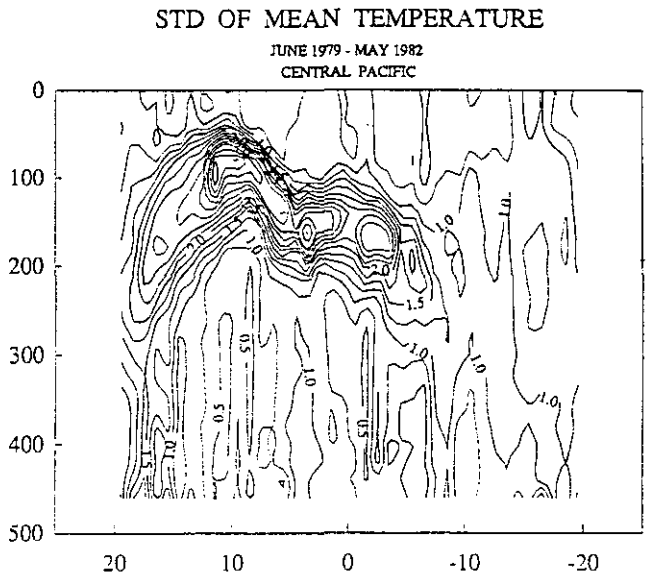

Figure 2C

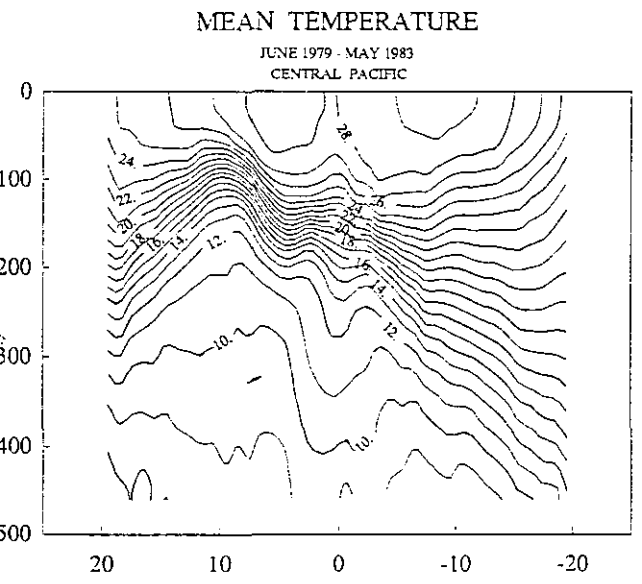

Figure 2D

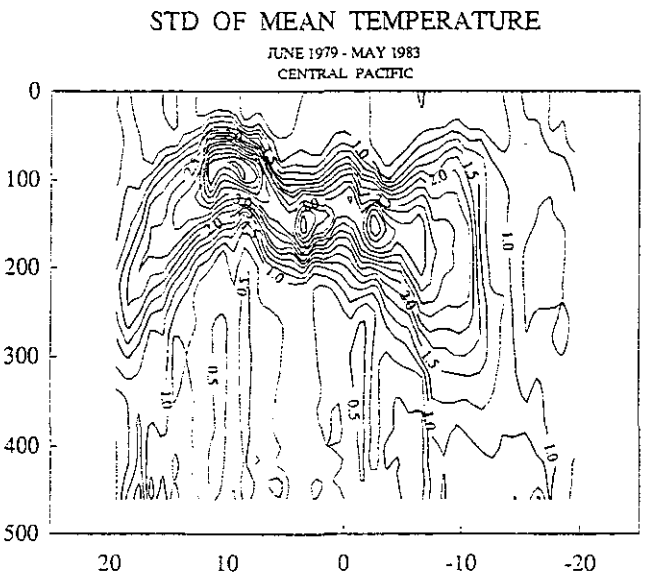

Figure 3A

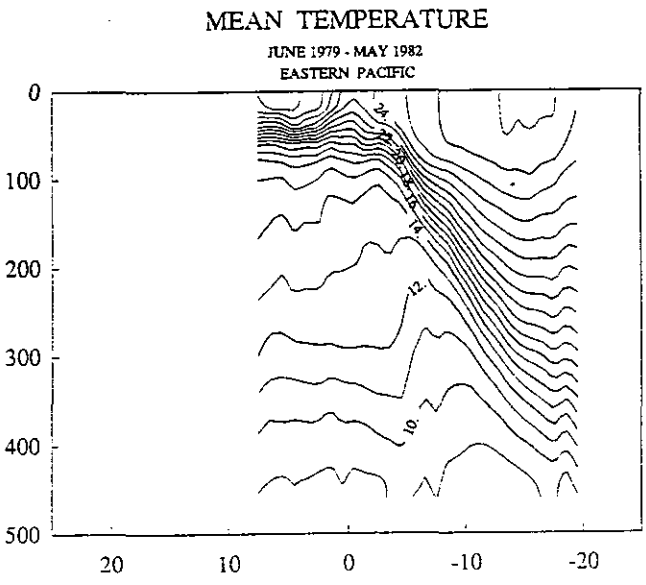

Figure 3B

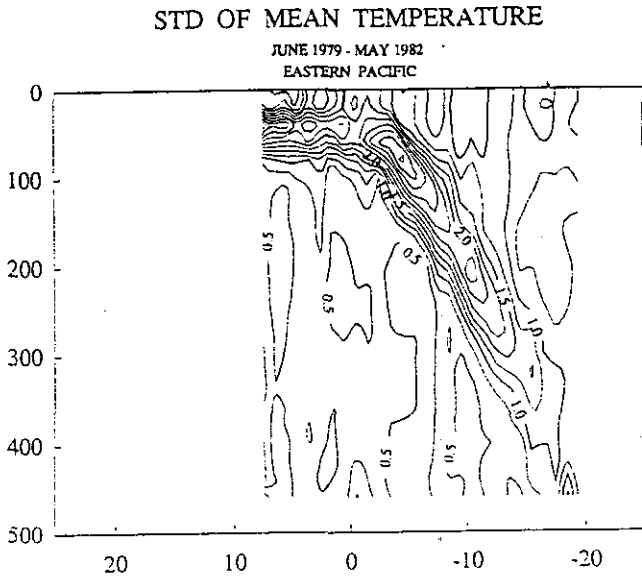

Figure 3C

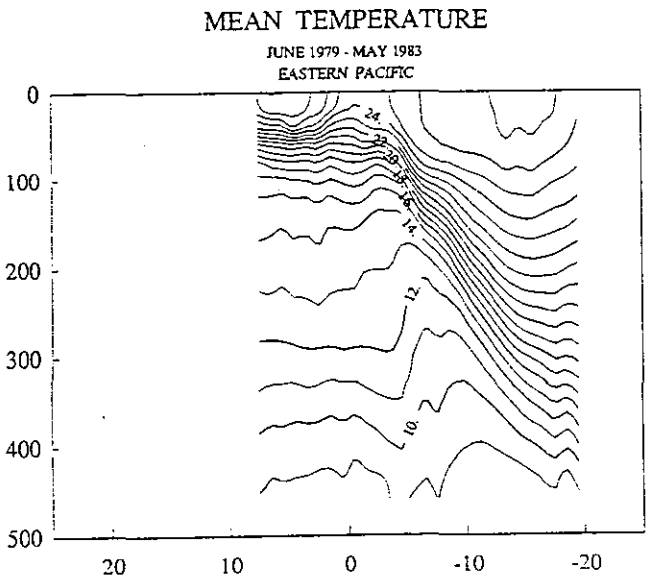

Figure 3D

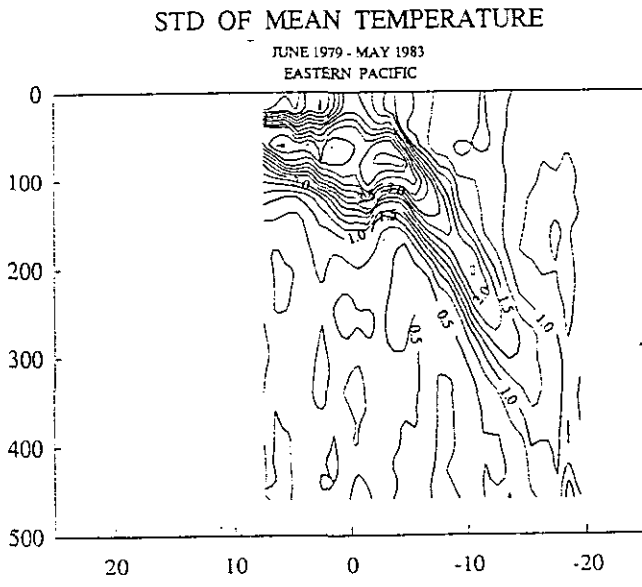

Figure 4A

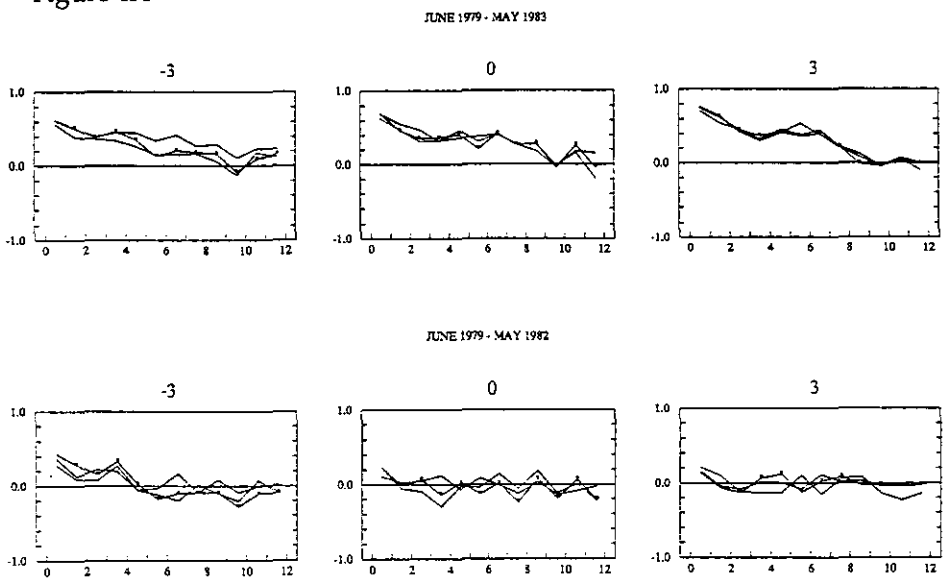

Figure 4B

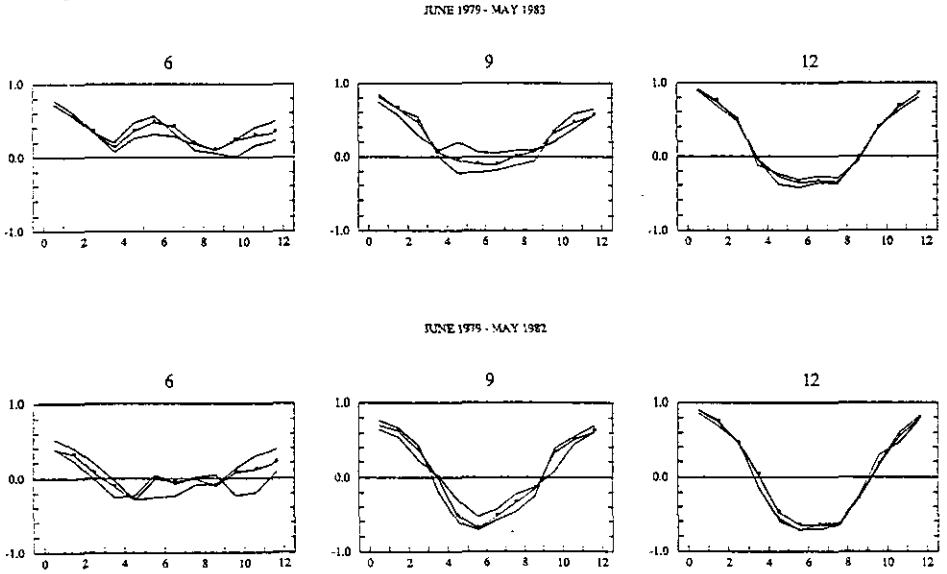

WESTERN PACIFIC
SEA SURFACE TEMPERATURE
TEMPORAL AUTOCORRELATION FUNCTION

Figure 4C

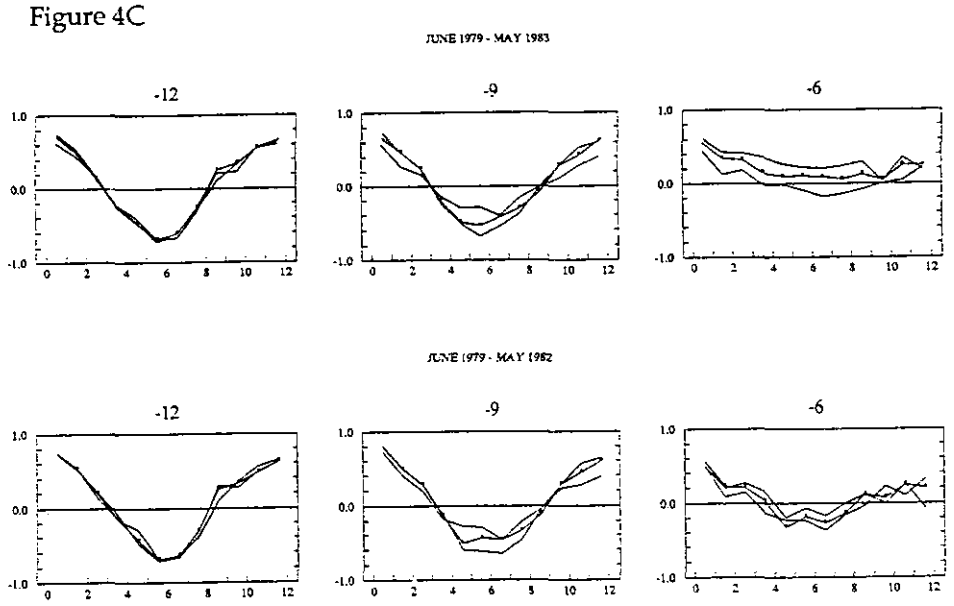

Figure 4D

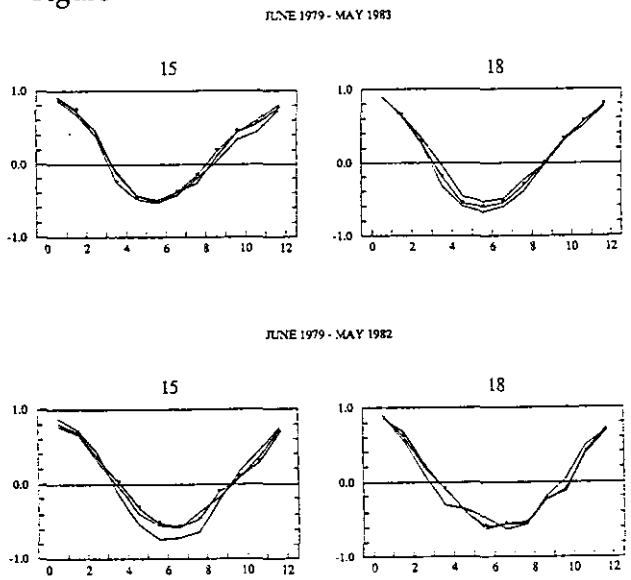

Figure 4E

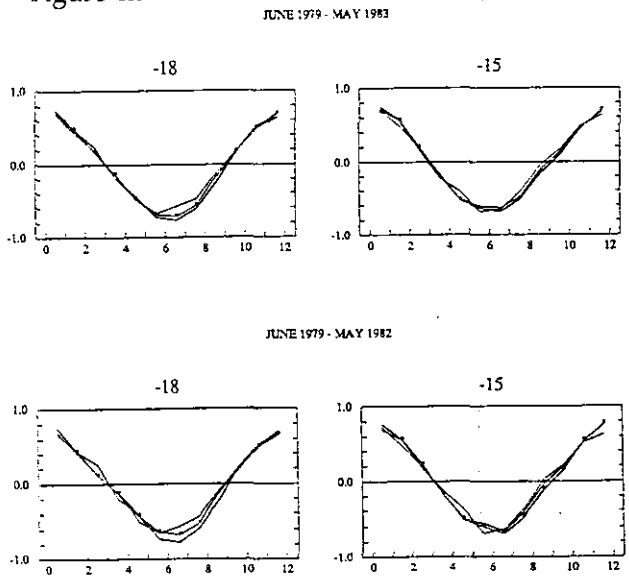

WESTERN PACIFIC
SEA SURFACE TEMPERATURE
TEMPORAL AUTOCORRELATION FUNCTION

Figure 5A

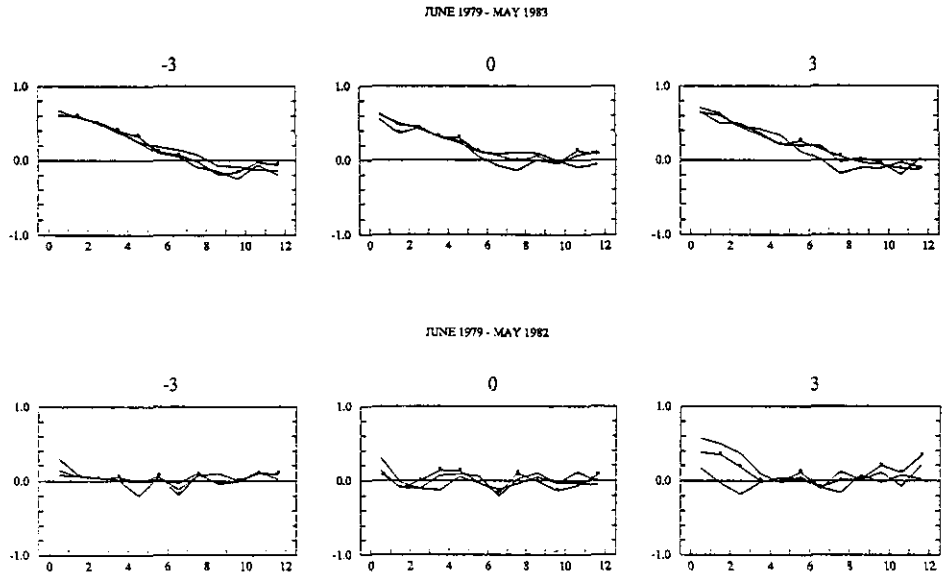

Figure 5B

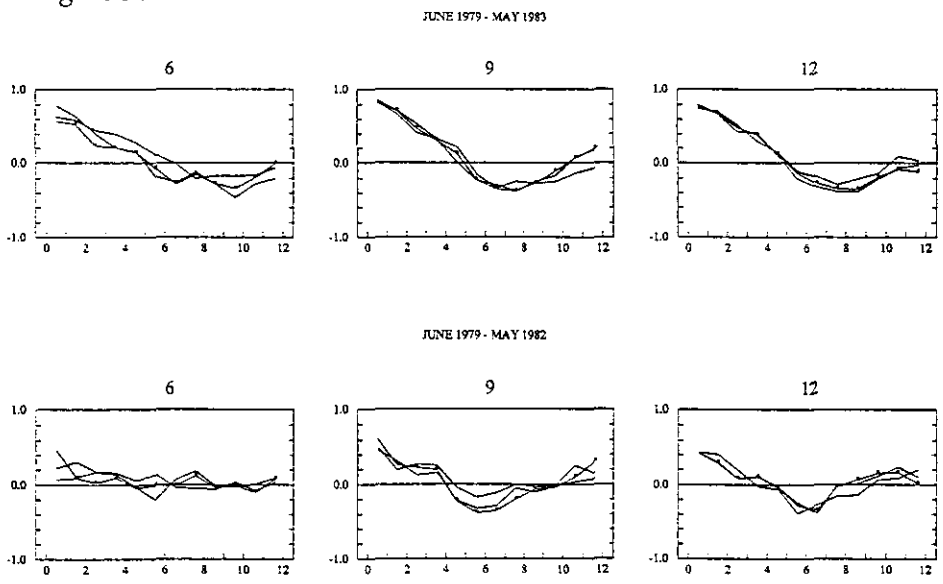

WESTERN PACIFIC
DEPTH OF 20 DEGREE ISOTHERM
TEMPORAL AUTOCORRELATION FUNCTION

Figure 5C

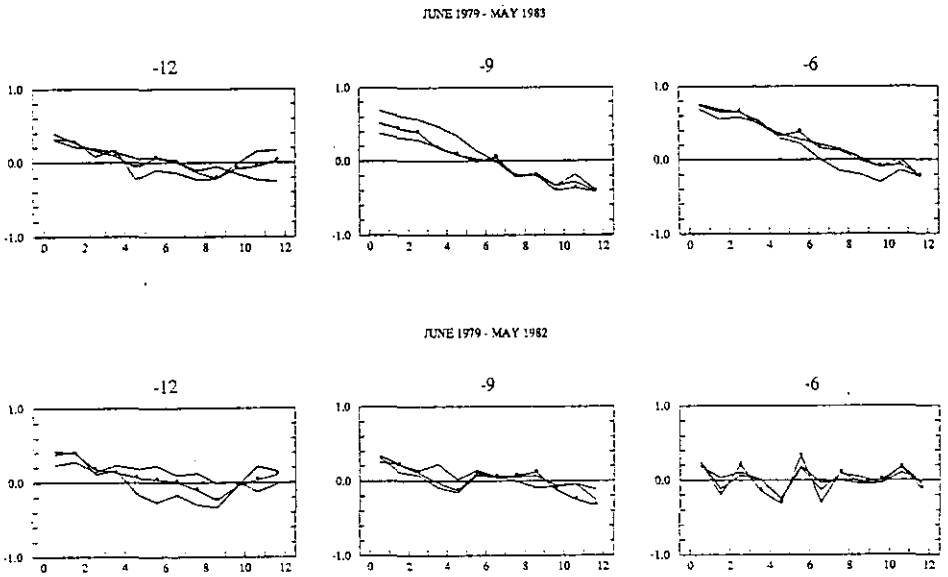

Figure 5D

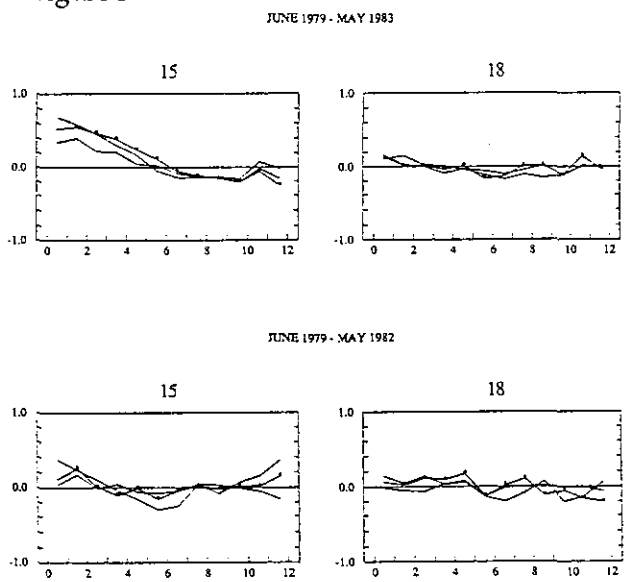

Figure 5E

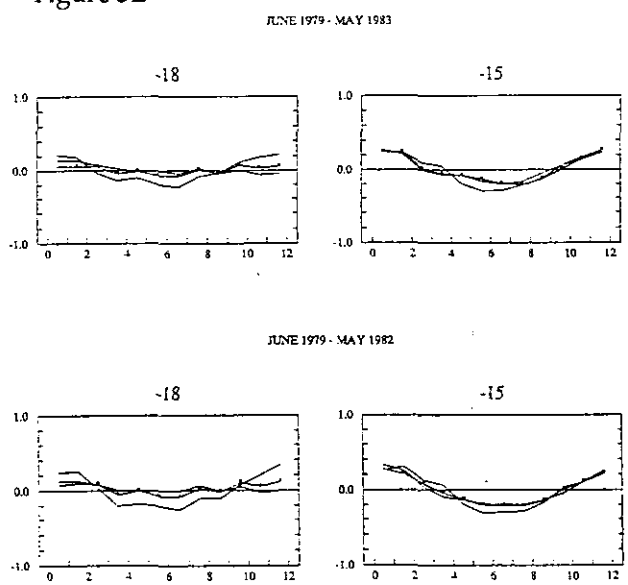

WESTERN PACIFIC
DEPTH OF 20 DEGREE ISOTHERM
TEMPORAL AUTOCORRELATION FUNCTION

Figure 6A

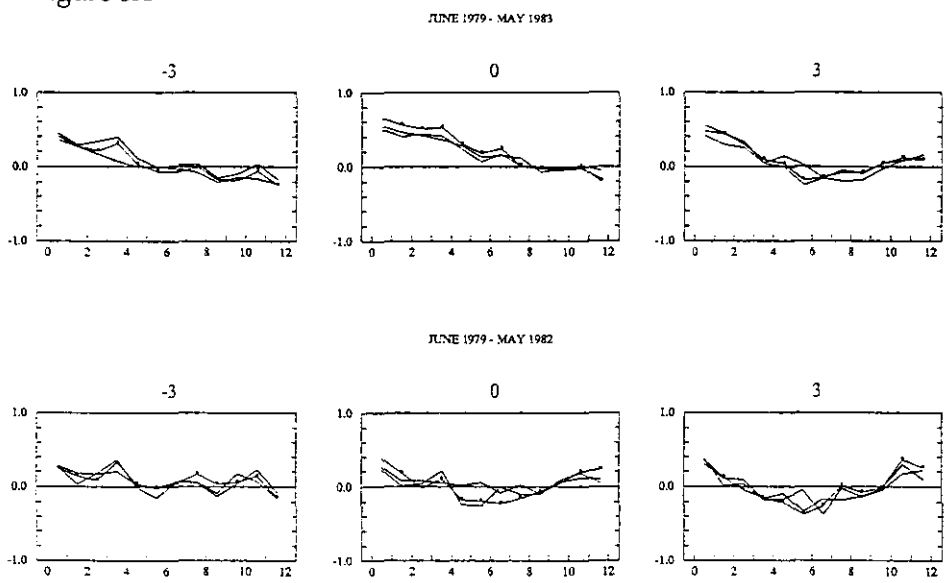

Figure 6B

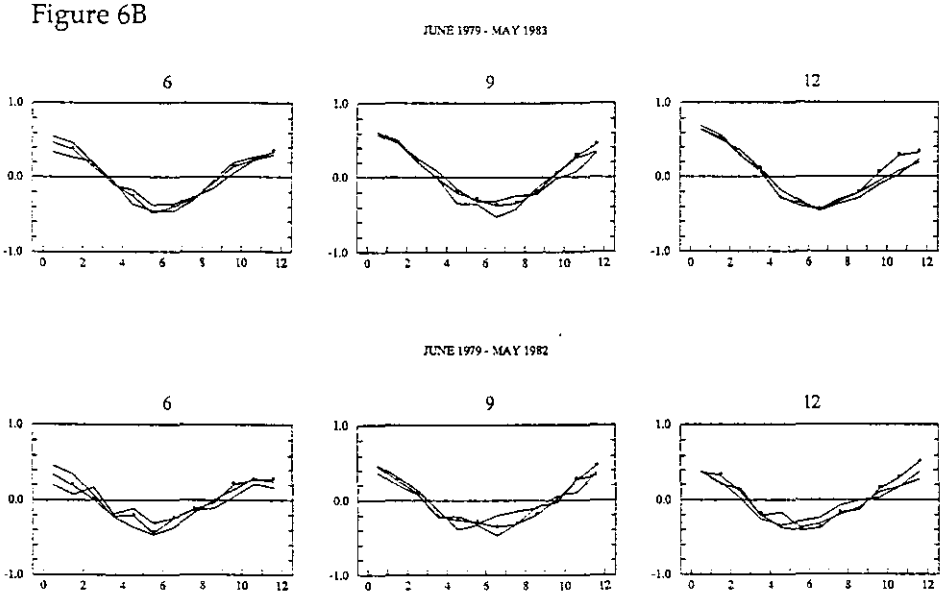

CENTRAL PACIFIC
SEA SURFACE TEMPERATURE
TEMPORAL AUTOCORRELATION FUNCTION

Figure 6C

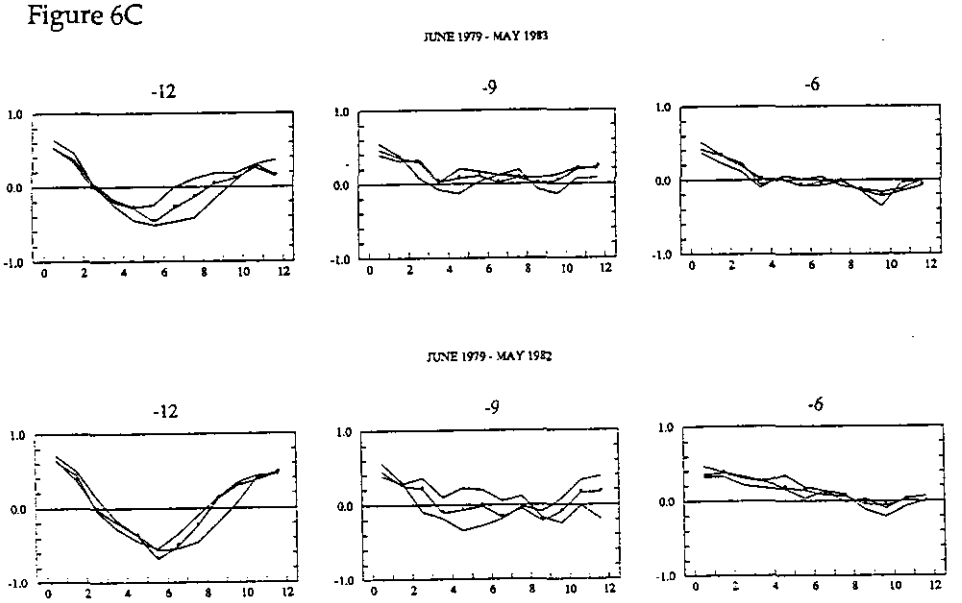

Figure 6D

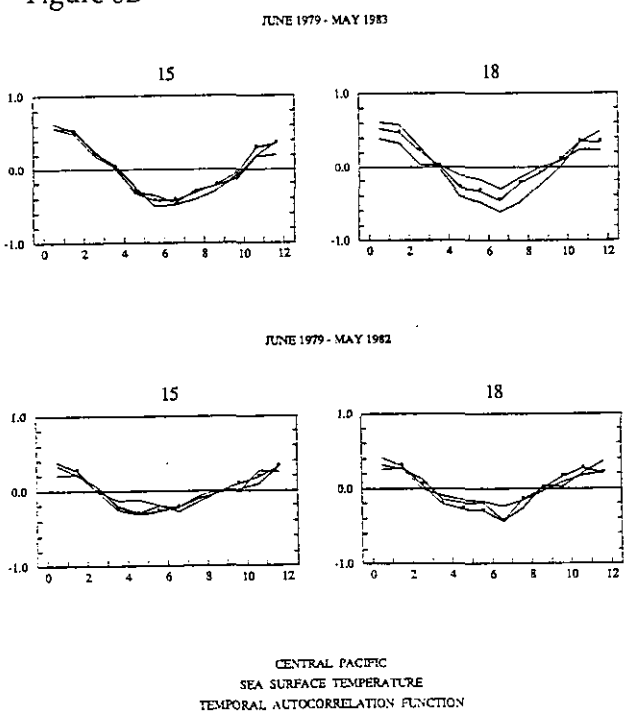

CENTRAL PACIFIC
SEA SURFACE TEMPERATURE
TEMPORAL AUTOCORRELATION FUNCTION

Figure 6E

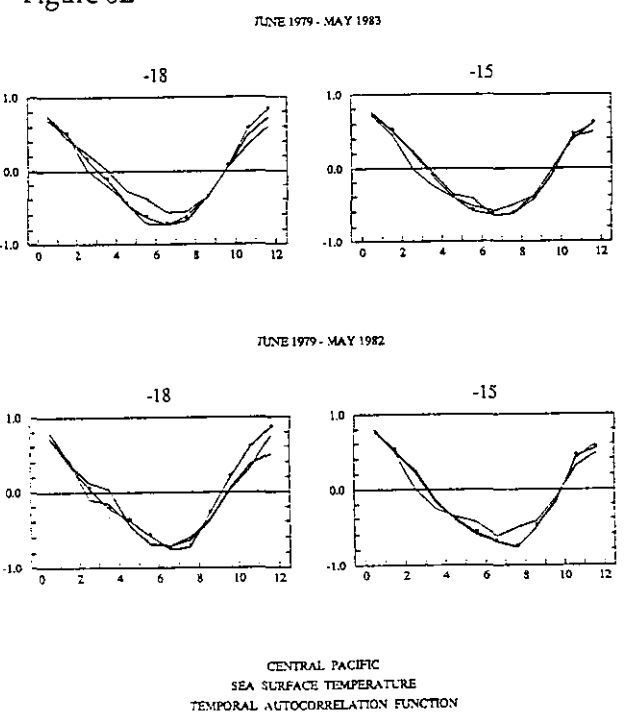

CENTRAL PACIFIC
SEA SURFACE TEMPERATURE
TEMPORAL AUTOCORRELATION FUNCTION

Figure 7A

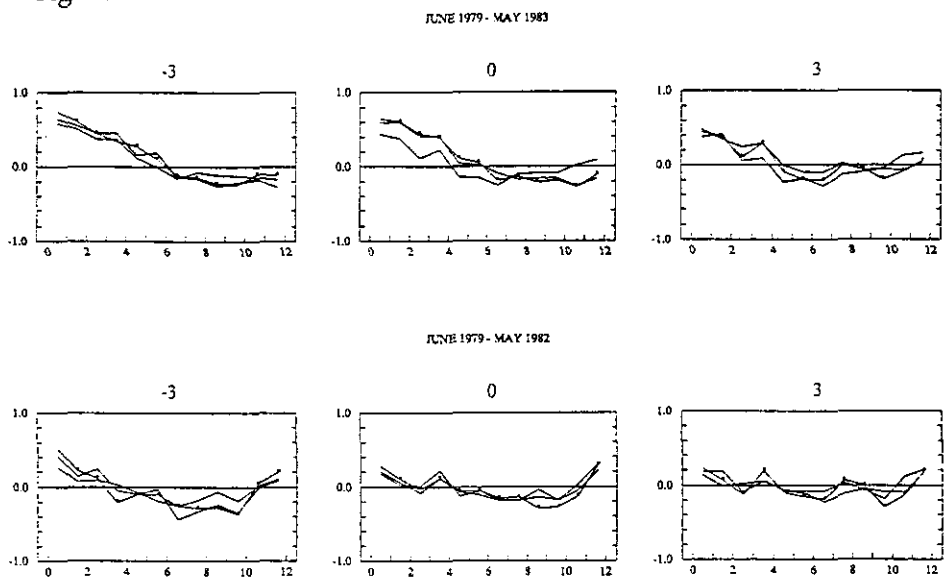

Figure 7B

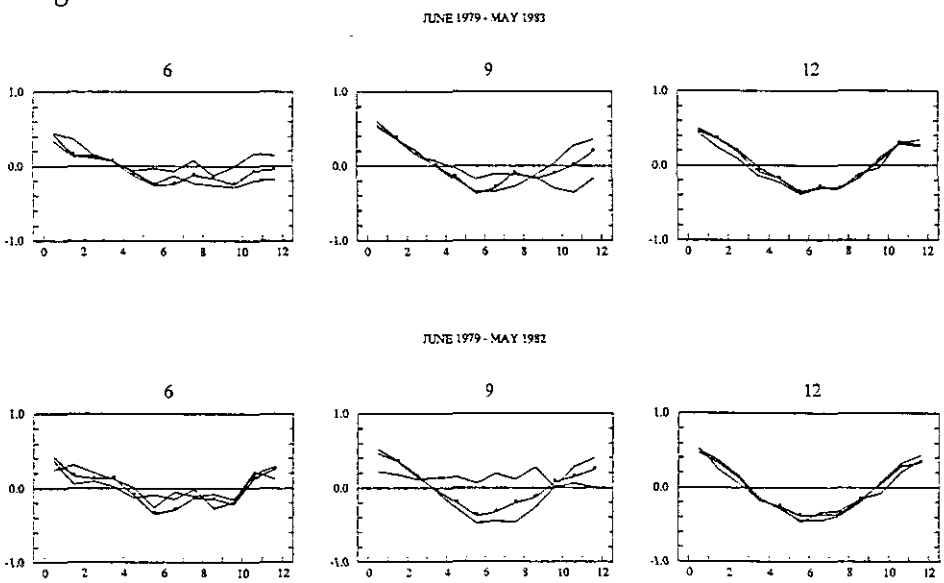

CENTRAL PACIFIC
DEPTH OF 20 DEGREE ISOTHERM
TEMPORAL AUTOCORRELATION FUNCTION

Figure 7C

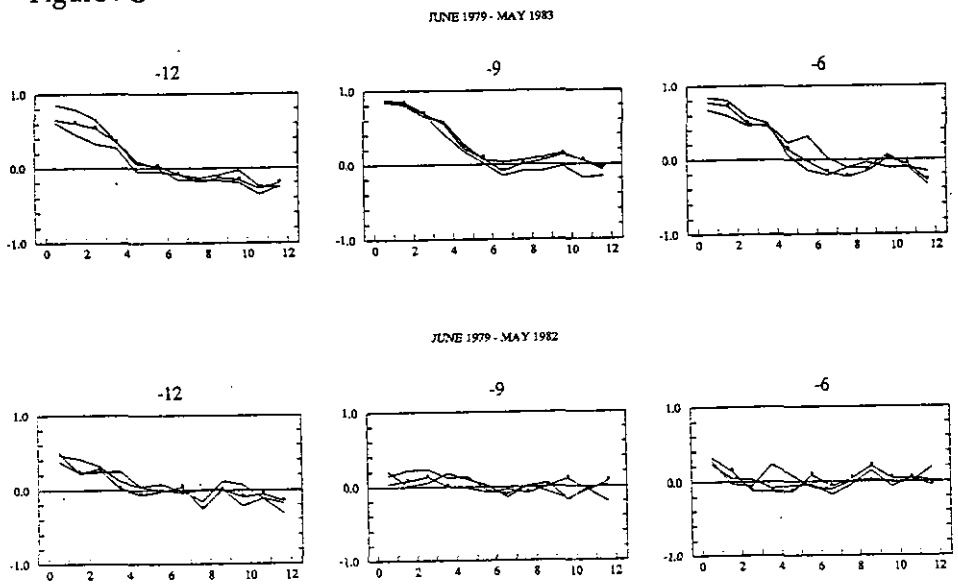

Figure 7D

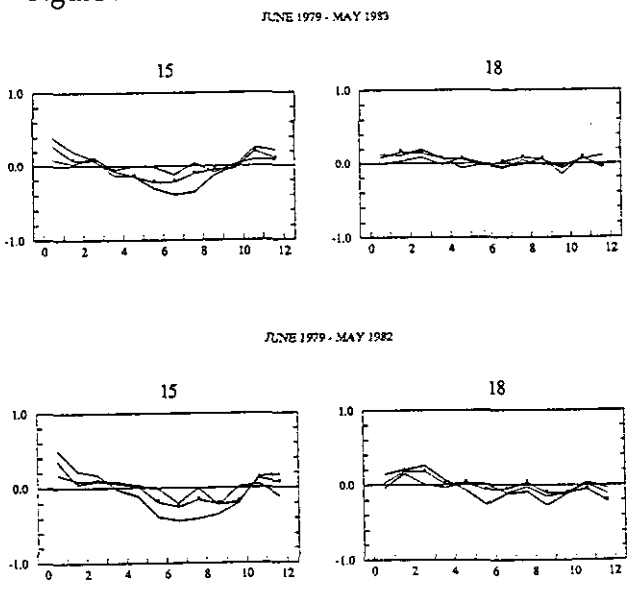

Figure 7E

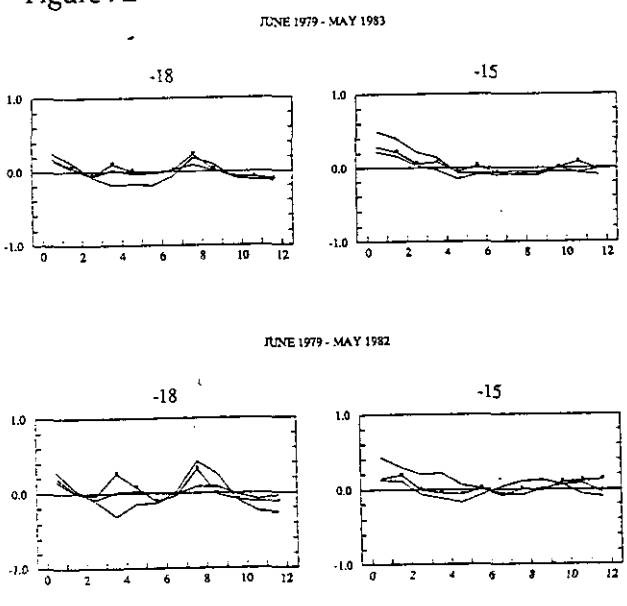

CENTRAL PACIFIC
DEPTH OF 20 DEGREE ISOTHERM
TEMPORAL AUTOCORRELATION FUNCTION

Figure 8A

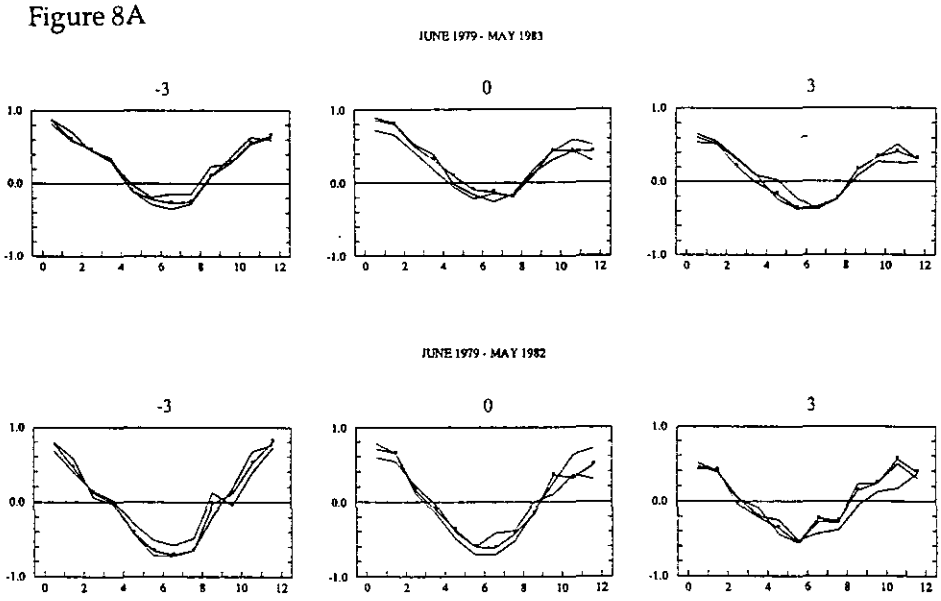

Figure 8B

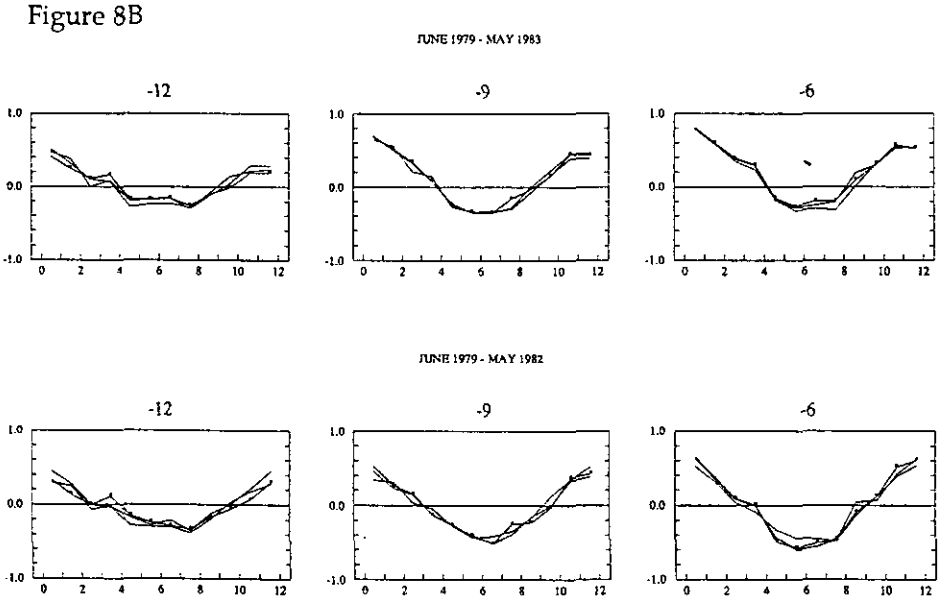

Figure 8C

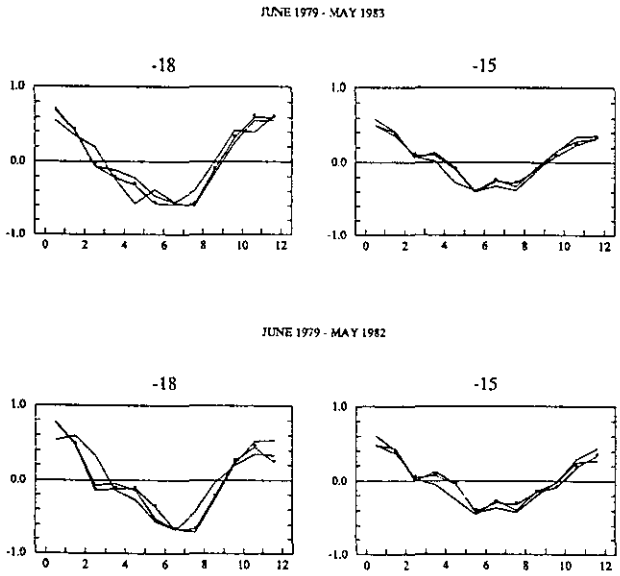

EASTERN PACIFIC
SEA SURFACE TEMPERATURE
TEMPORAL AUTOCORRELATION FUNCTION

Figure 9A

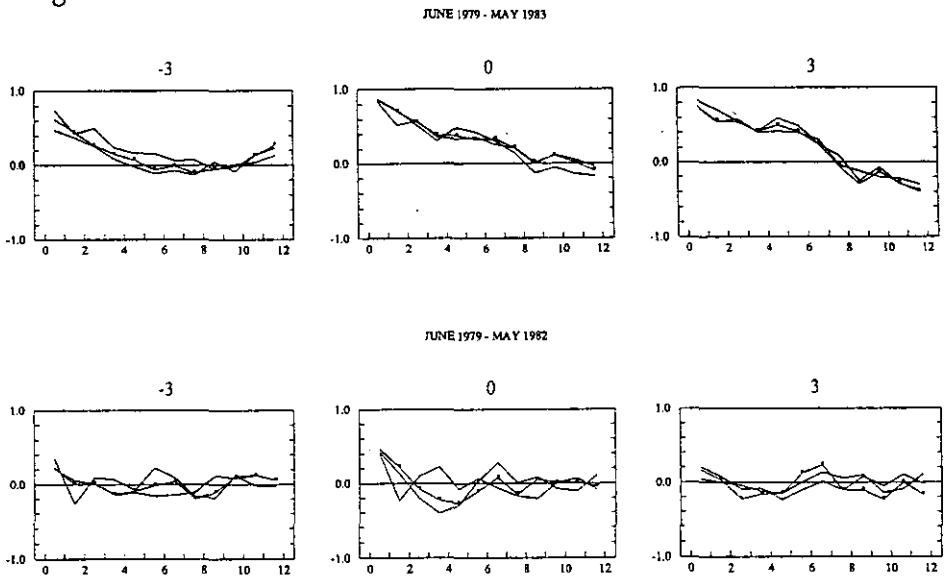

Figure 9B

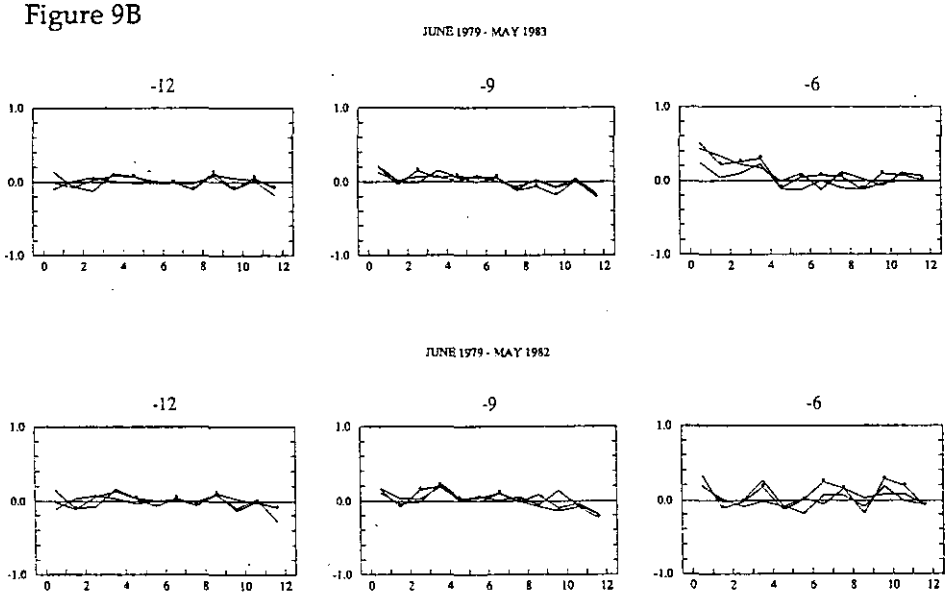

Figure 9C

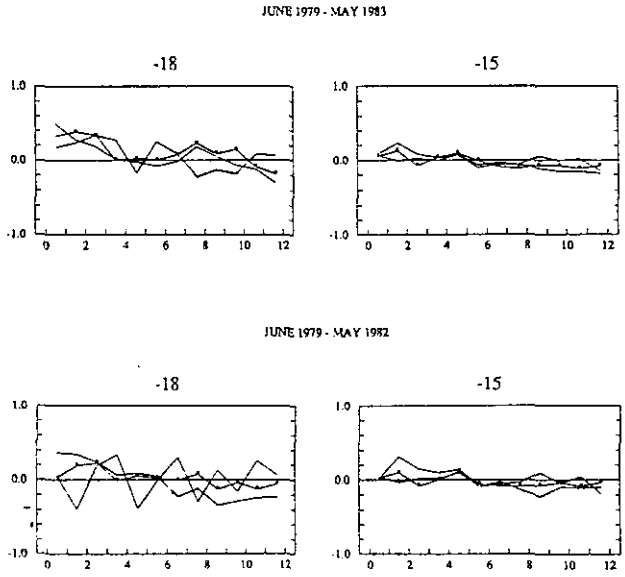

EASTERN PACIFIC
DEPTH OF 20 DEGREE ISOTHERM
TEMPORAL AUTOCORRELATION FUNCTION

Figure 10A

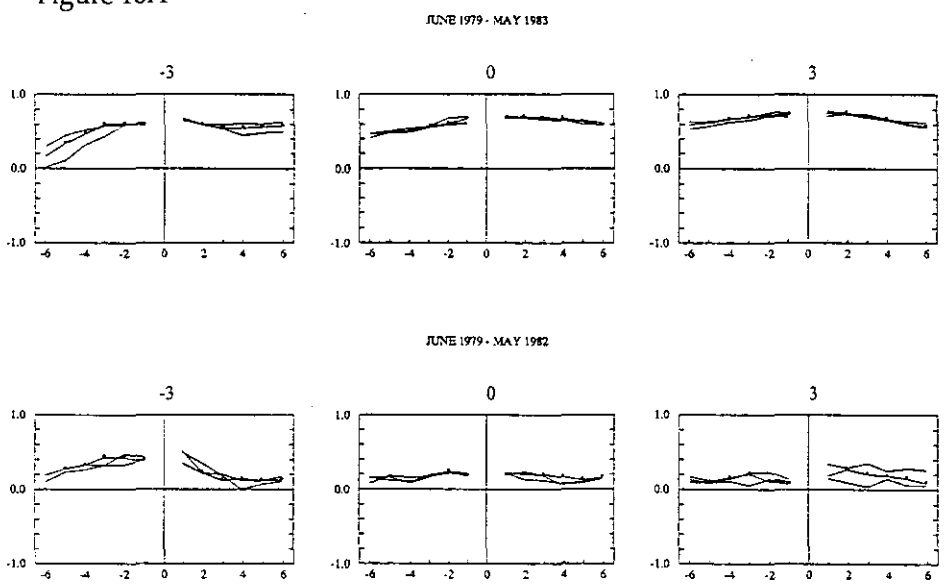

Figure 10B

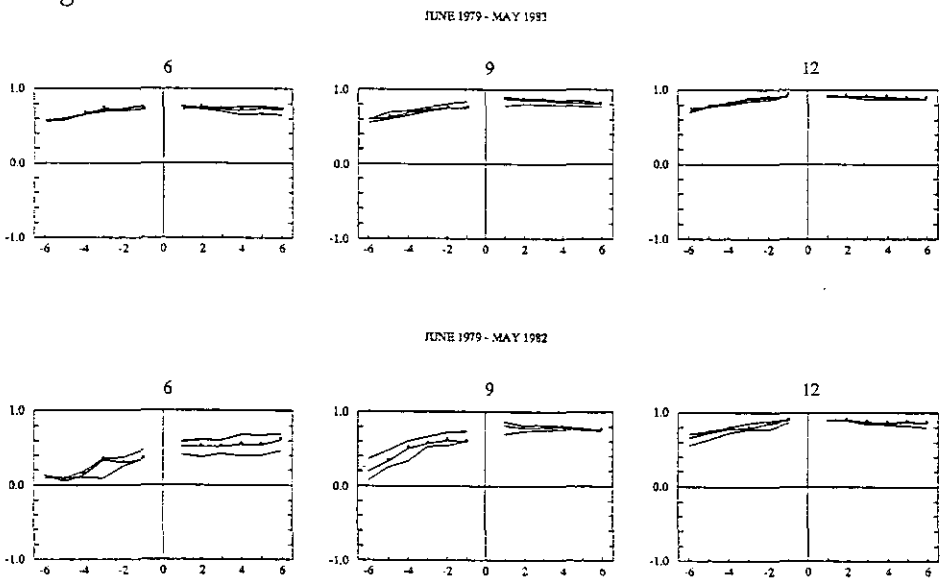

WESTERN PACIFIC
SEA SURFACE TEMPERATURE
MERIDIONAL AUTOCORRELATION FUNCTION

Figure 10C

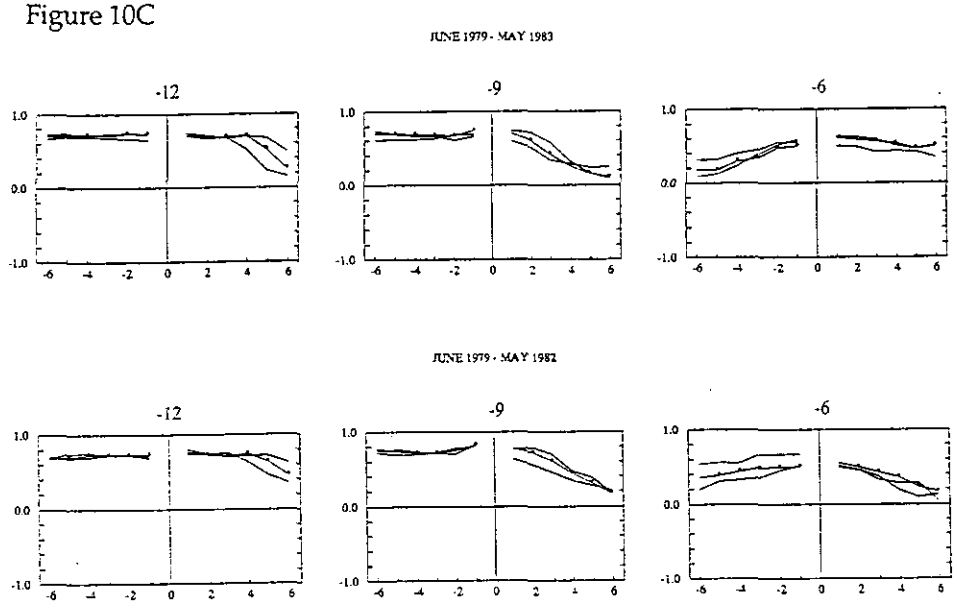

Figure 10D

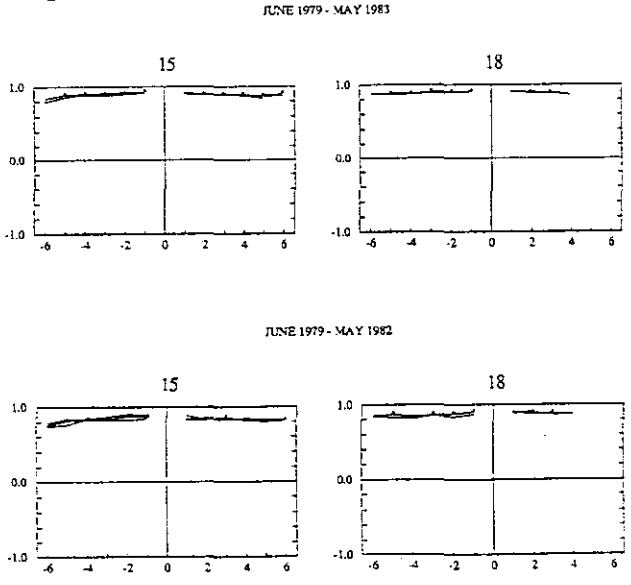

Figure 10E

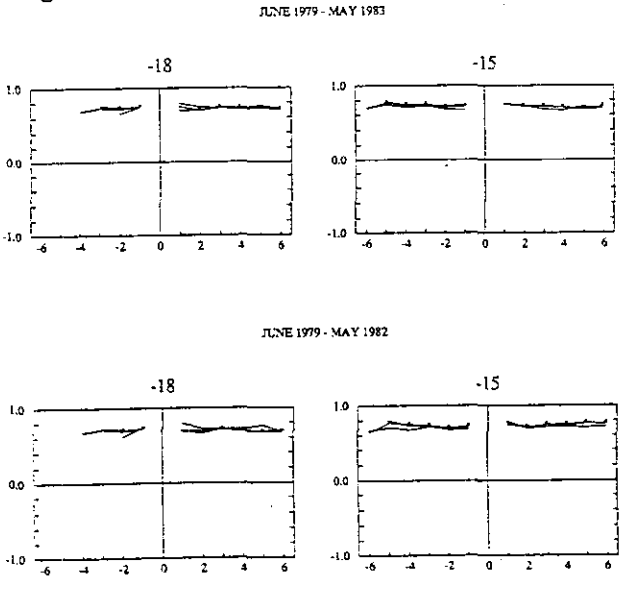

WESTERN PACIFIC
SEA SURFACE TEMPERATURE
MERIDIONAL AUTOCORRELATION FUNCTION

Figure 11A

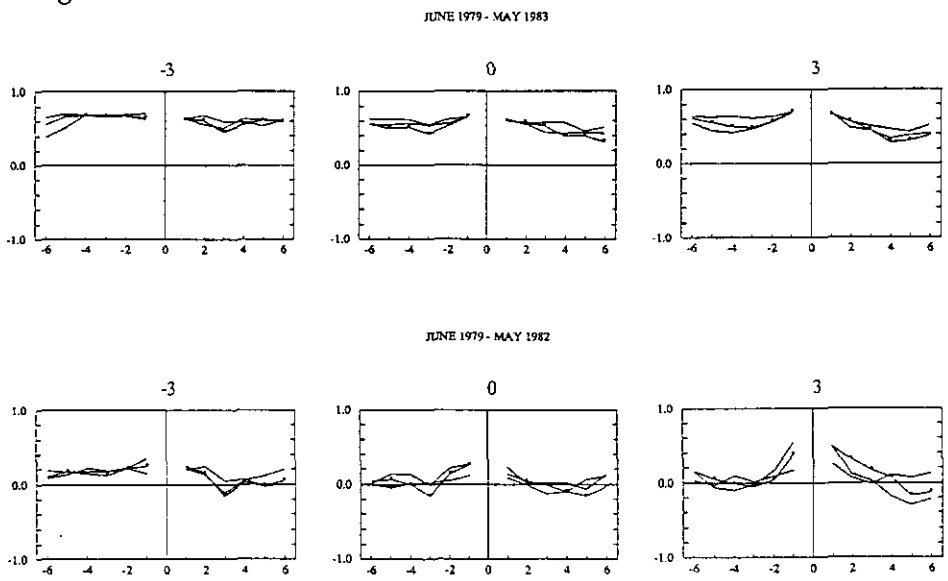

Figure 11B

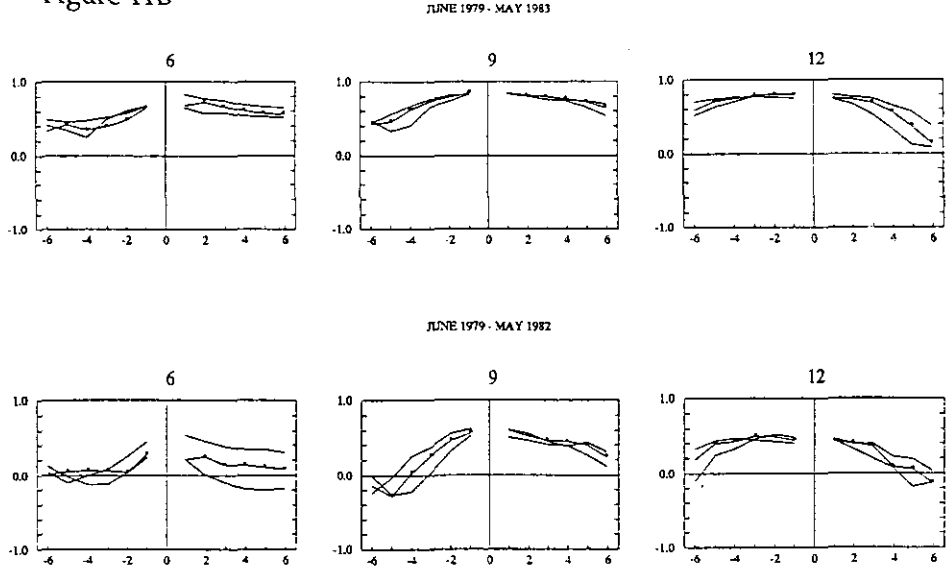

WESTERN PACIFIC
DEPTH OF 20 DEGREE ISOTHERM
MERIDIONAL AUTOCORRELATION FUNCTION

Figure 11C

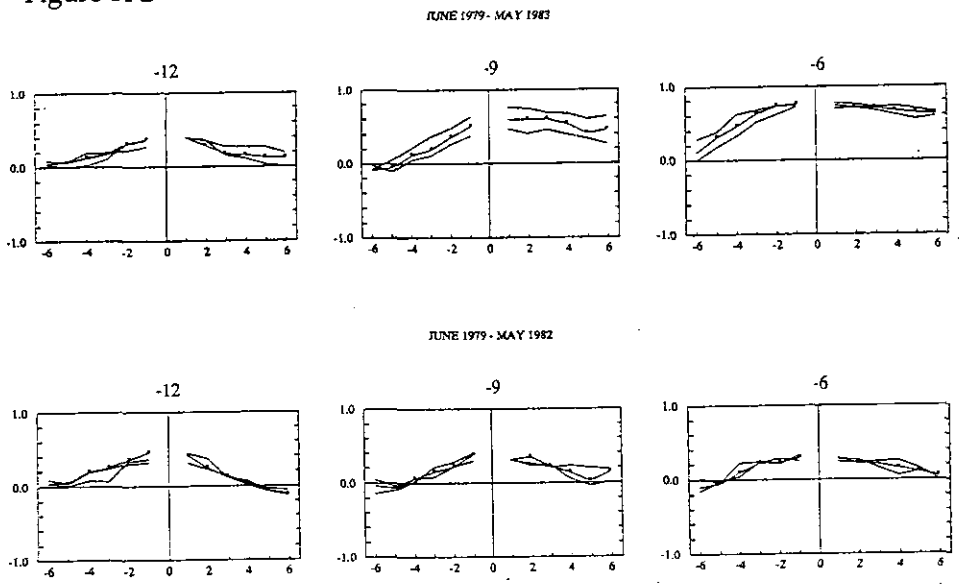

Figure 11D

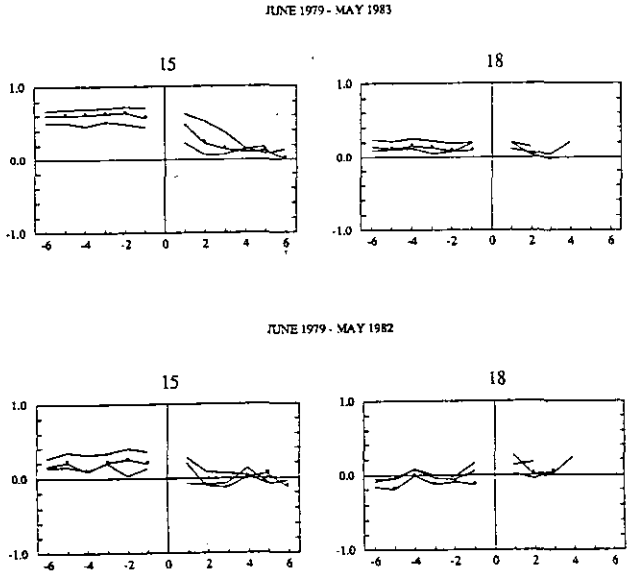

Figure 11E

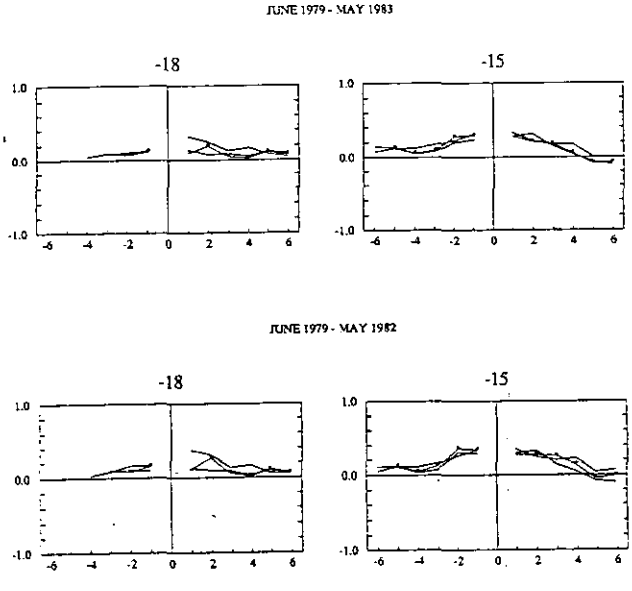

WESTERN PACIFIC
DEPTH OF 20 DEGREE ISOTHERM
MERIDIONAL AUTOCORRELATION FUNCTION

Figure 12A

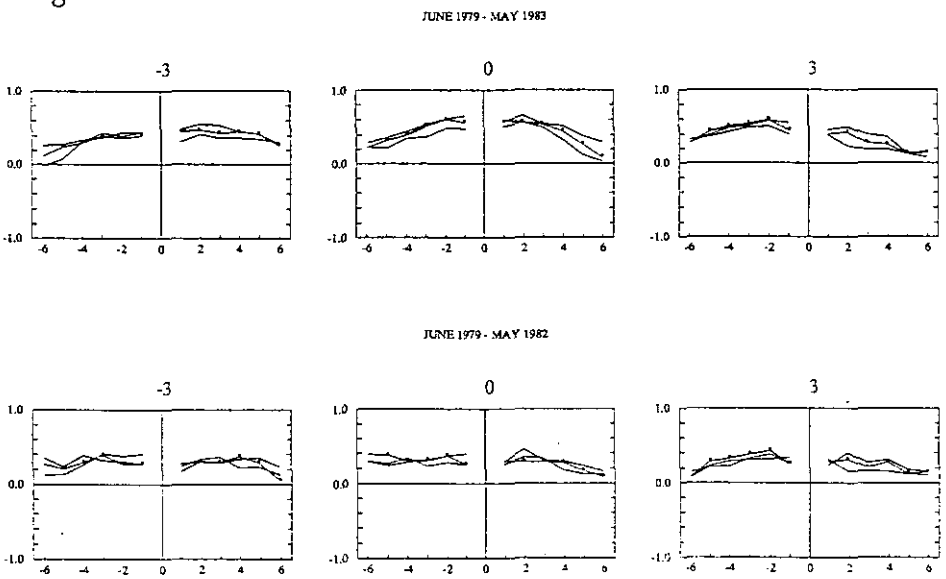

Figure 12B

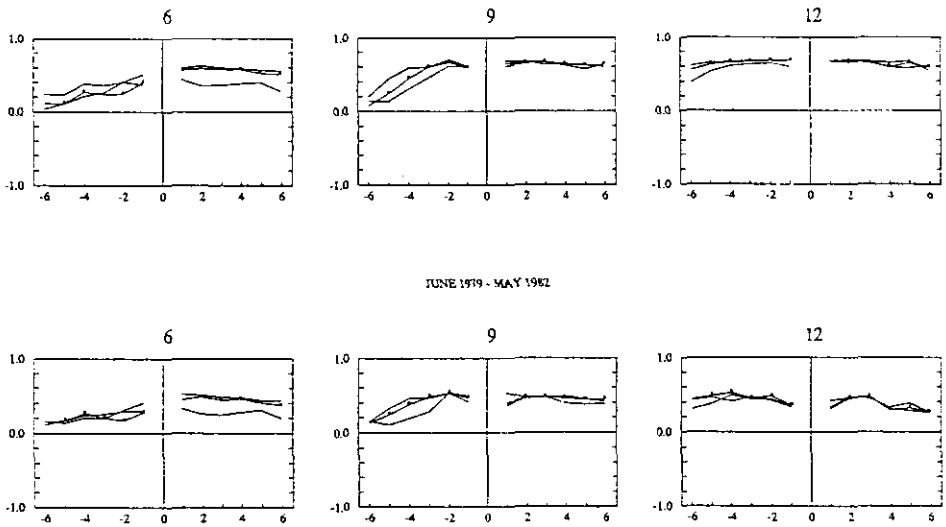

CENTRAL PACIFIC
SEA SURFACE TEMPERATURE
MERIDIONAL AUTOCORRELATION FUNCTION

Figure 12C

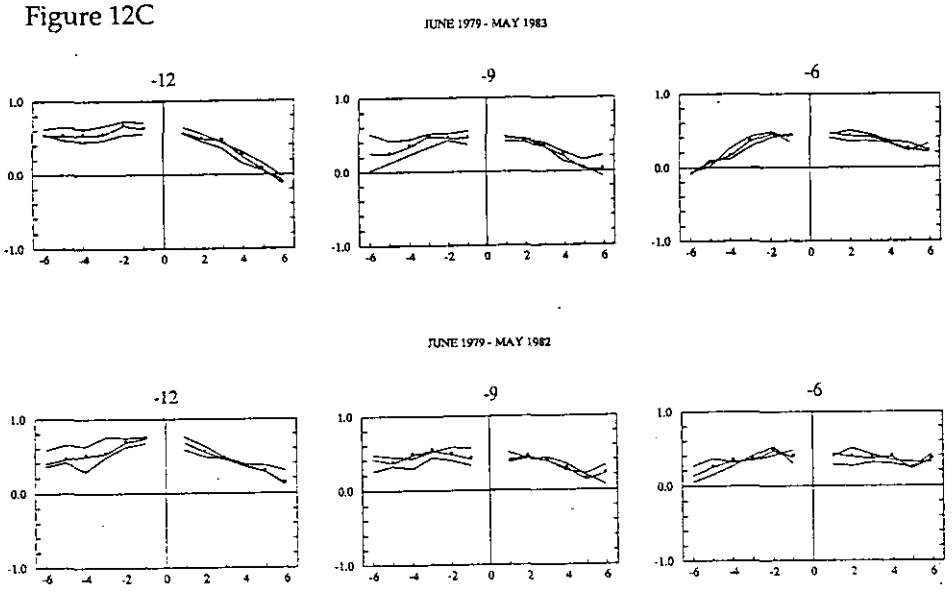

Figure 12D

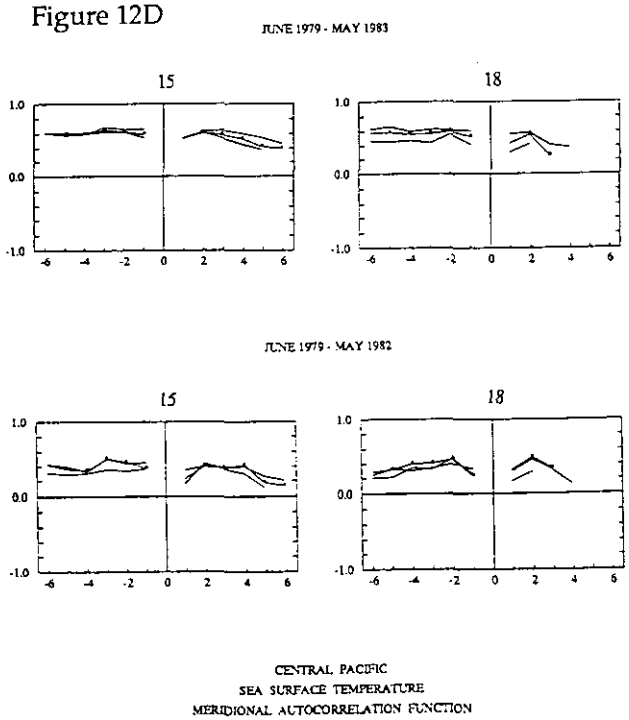

CENTRAL PACIFIC
SEA SURFACE TEMPERATURE
MERIDIONAL AUTOCORRELATION FUNCTION

Figure 12E

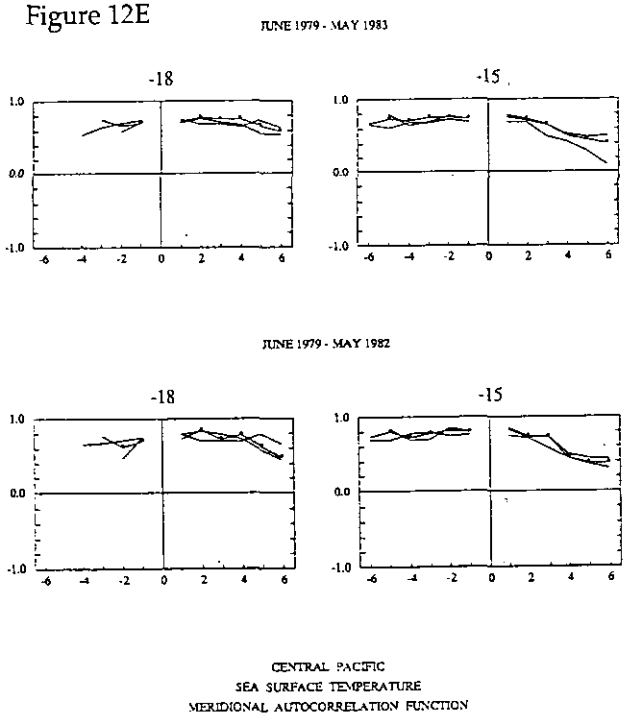

CENTRAL PACIFIC
SEA SURFACE TEMPERATURE
MERIDIONAL AUTOCORRELATION FUNCTION

Figure 13A

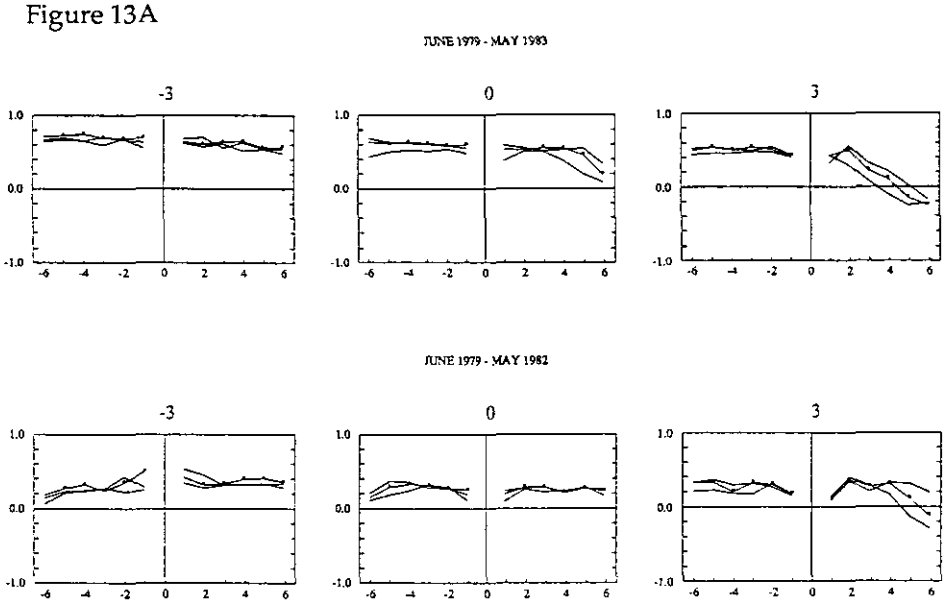

Figure 13B

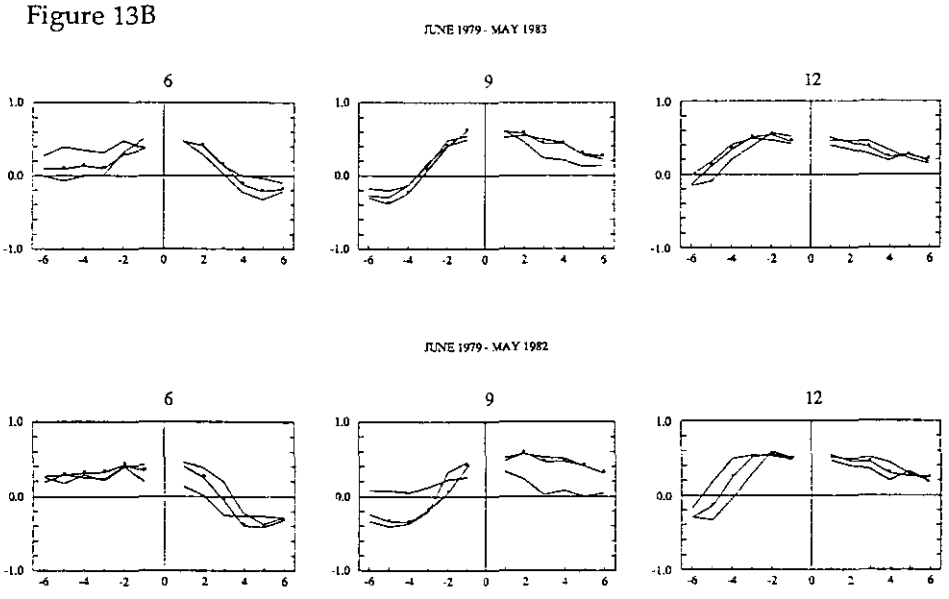

CENTRAL PACIFIC
DEPTH OF 20 DEGREE ISOTHERM
MERIDIONAL AUTOCORRELATION FUNCTION

Figure 13C

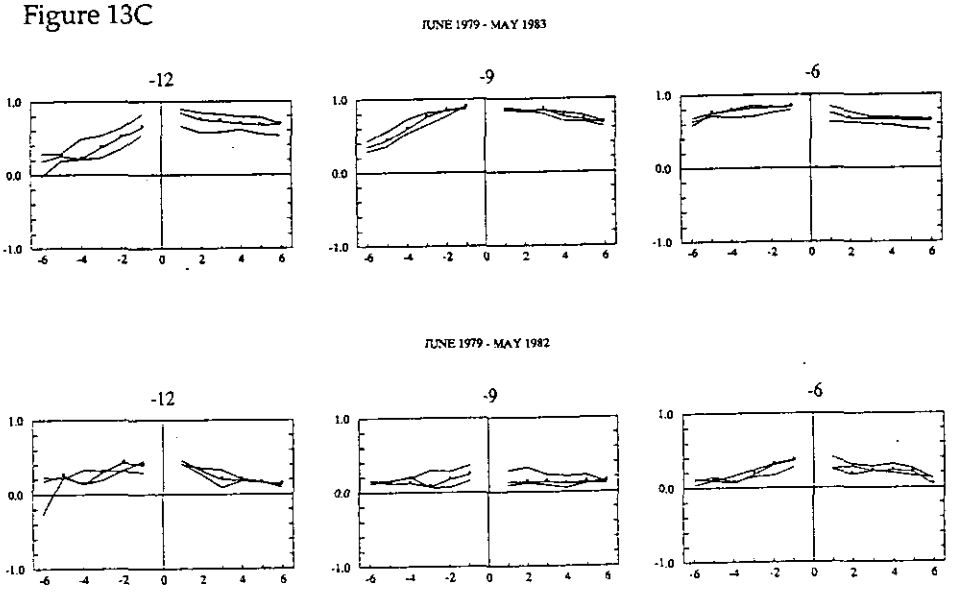

Figure 13D

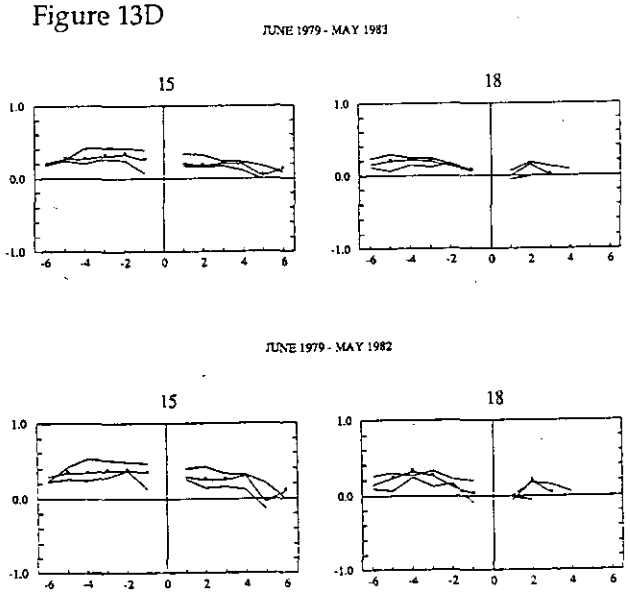

Figure 13E

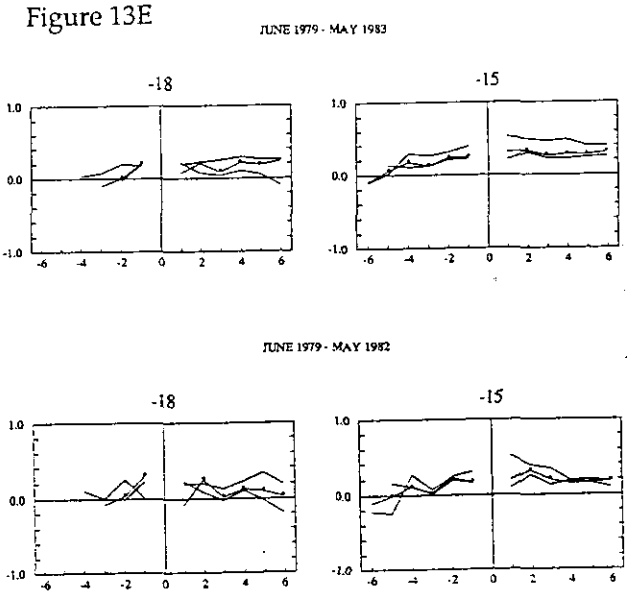

CENTRAL PACIFIC
DEPTH OF 20 DEGREE ISOTHERM
MERIDIONAL AUTOCORRELATION FUNCTION

Figure 14A

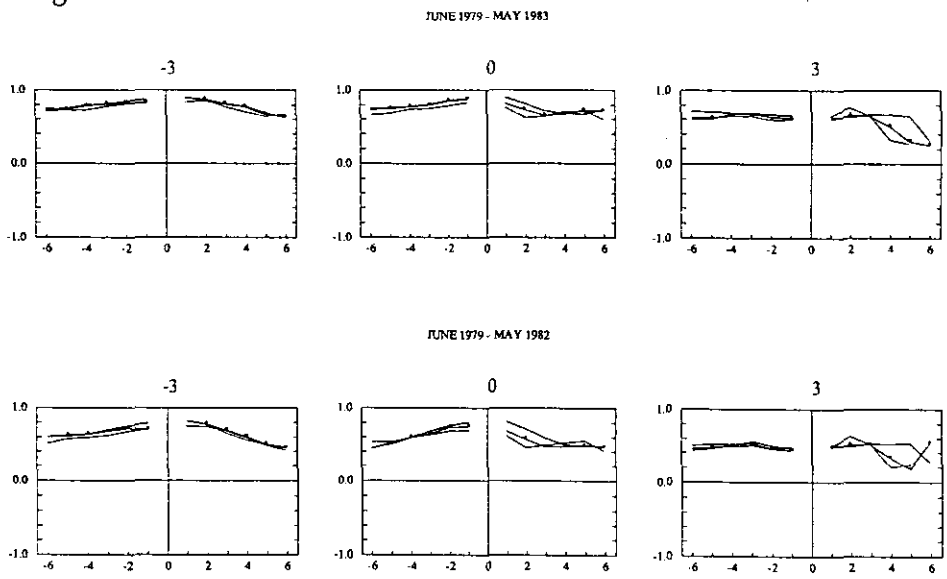

Figure 14B

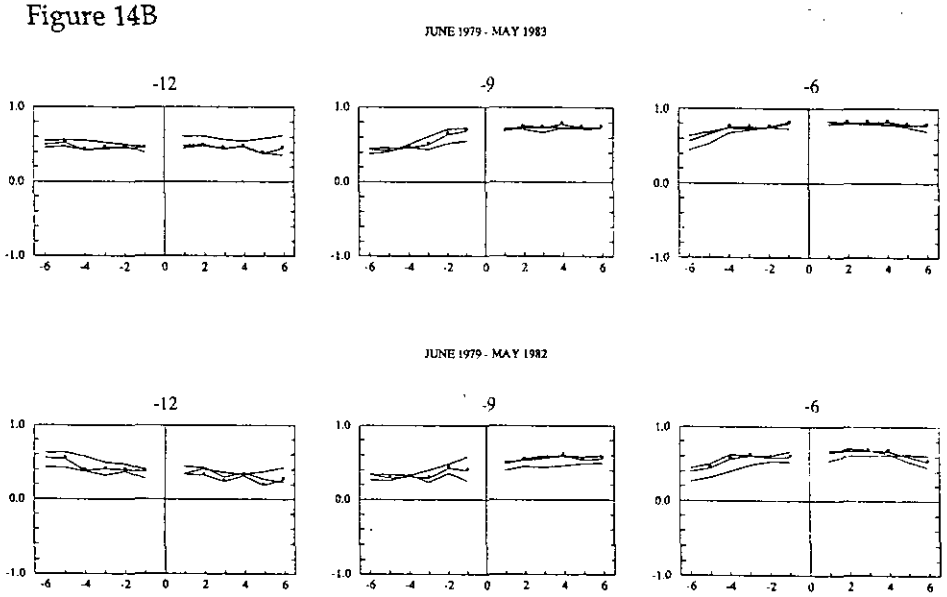

Figure 14C

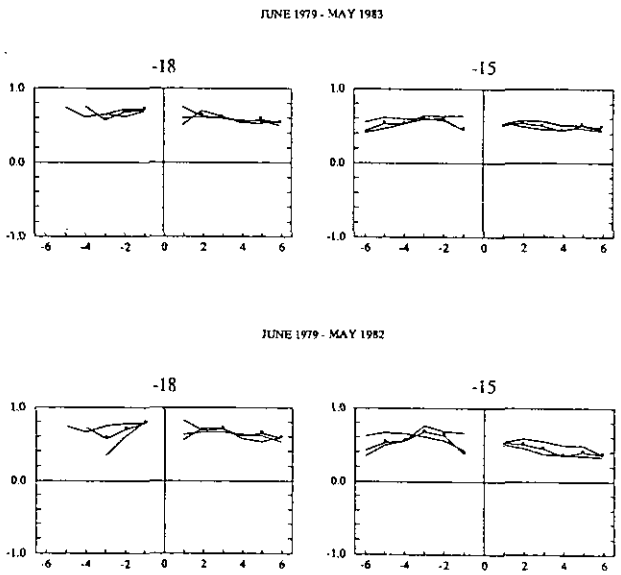

EASTERN PACIFIC
SEA SURFACE TEMPERATURE
MERIDIONAL AUTOCORRELATION FUNCTION

Figure 15A

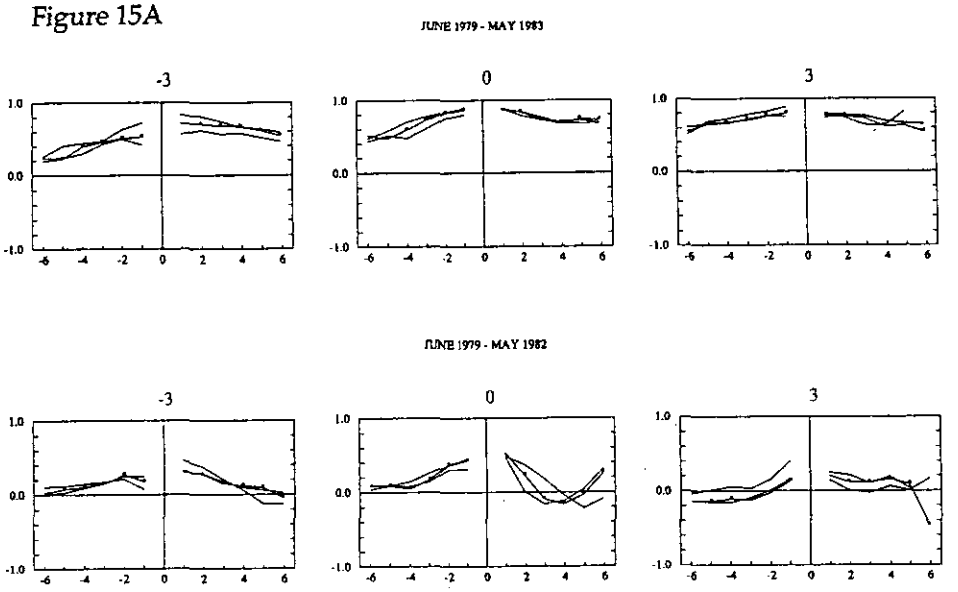

Figure 15B

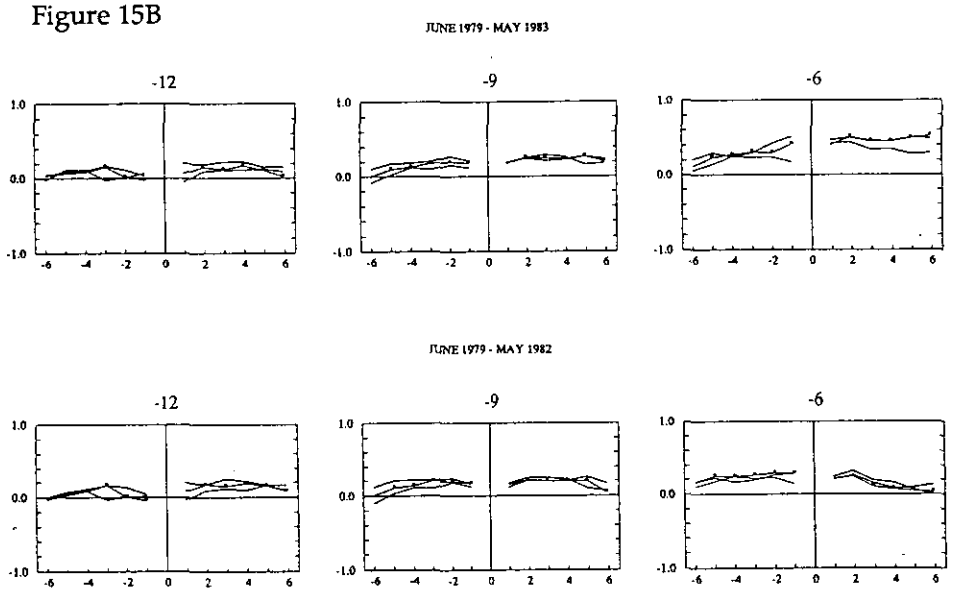

Figure 15C

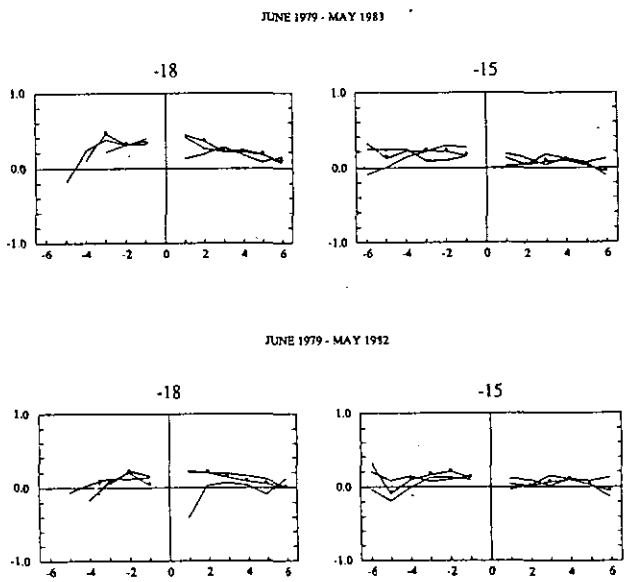

EASTERN PACIFIC
DEPTH OF 20 DEGREE ISOTHERM
MERIDIONAL AUTOCORRELATION FUNCTION

SST TEMPORAL SIGNAL-TO-NOISE RATIO

Figure 16A

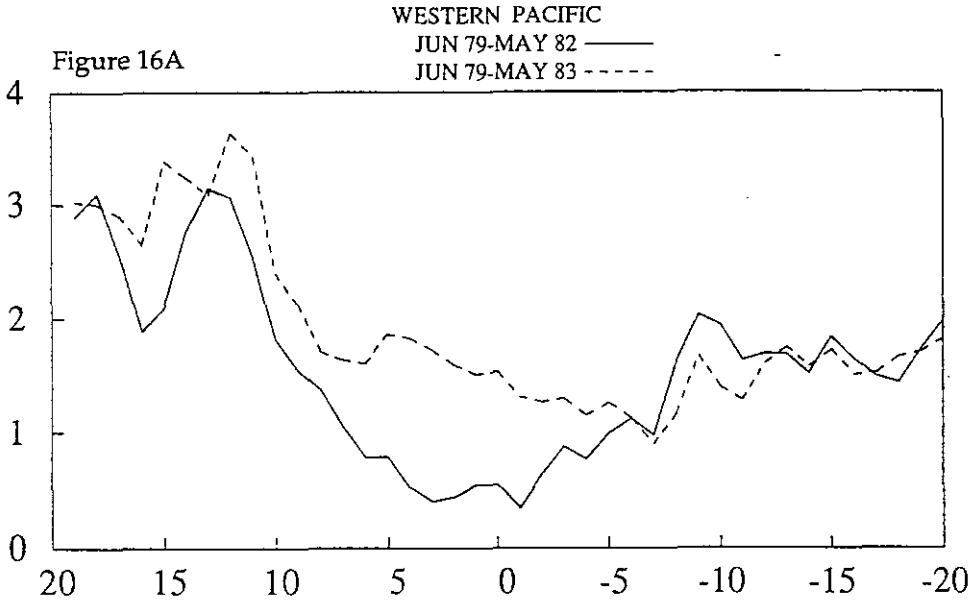

Figure 16B

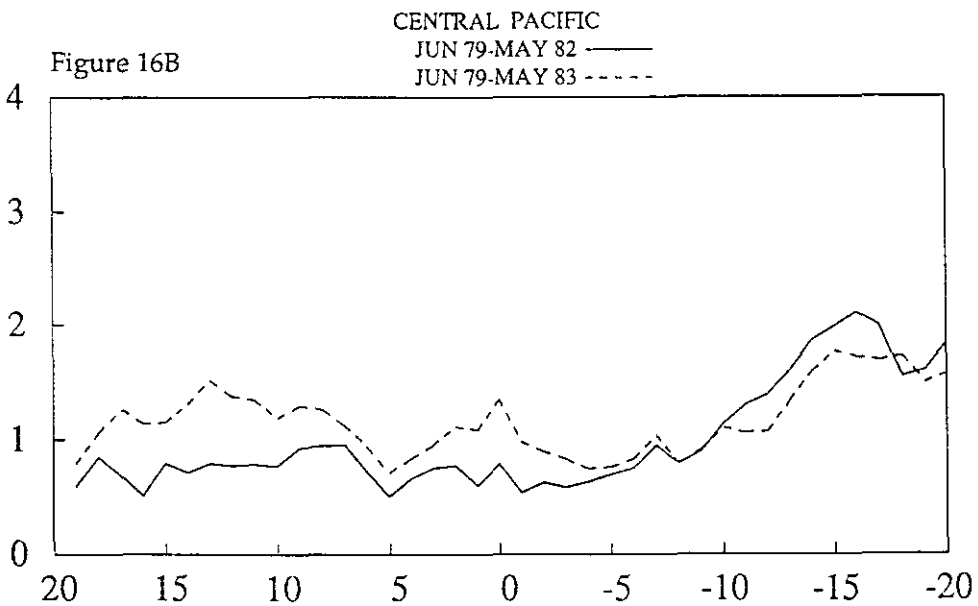

Figure 16C

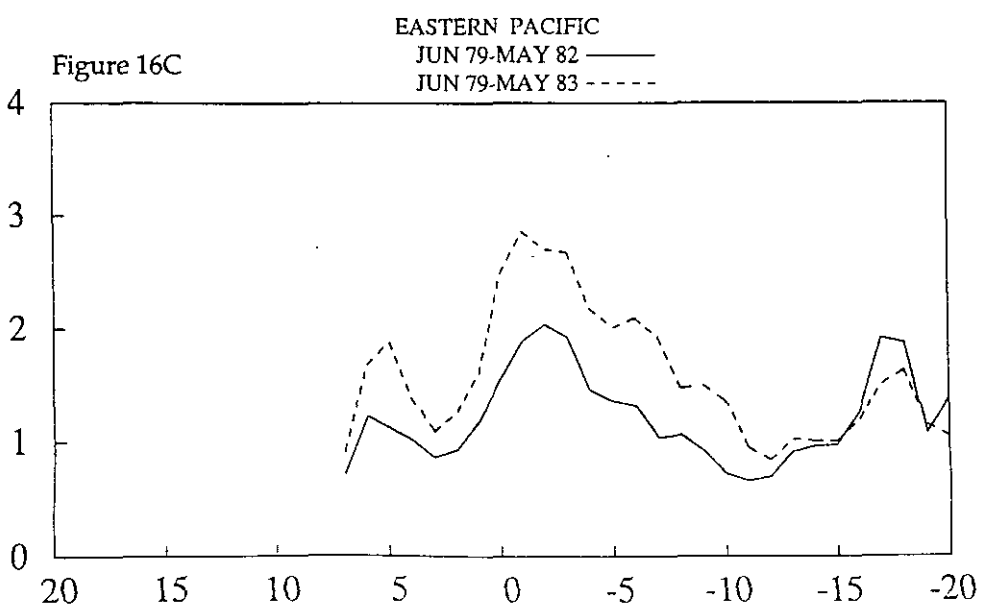

D20 TEMPORAL SIGNAL-TO-NOISE RATIO

Figure 17A

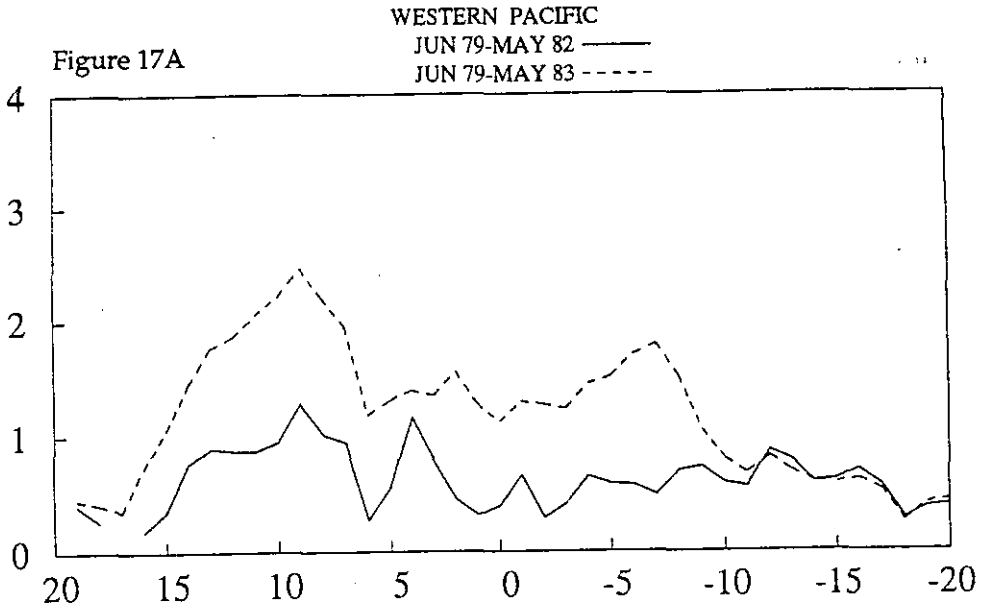

Figure 17B

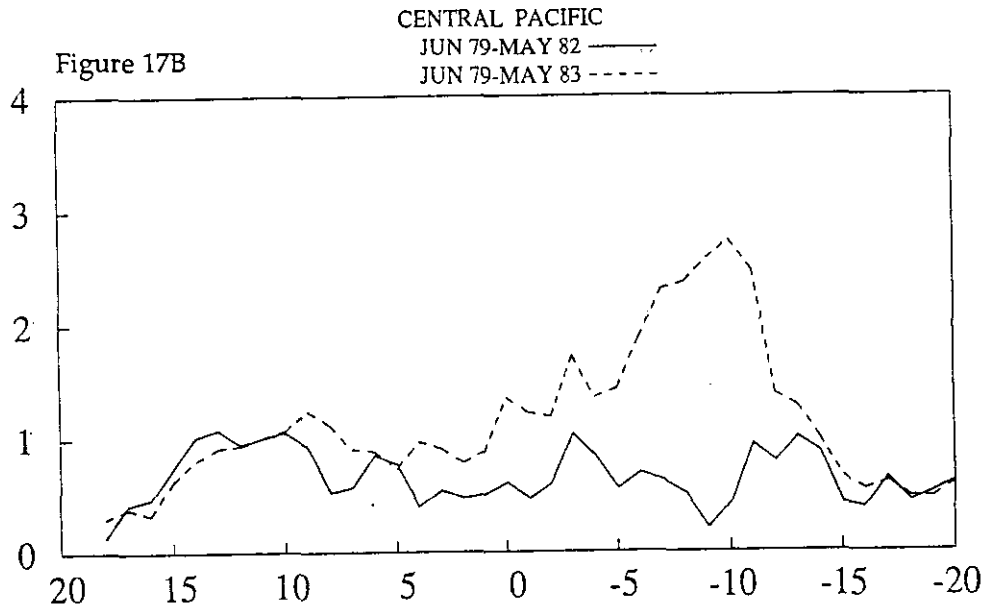

Figure 17C

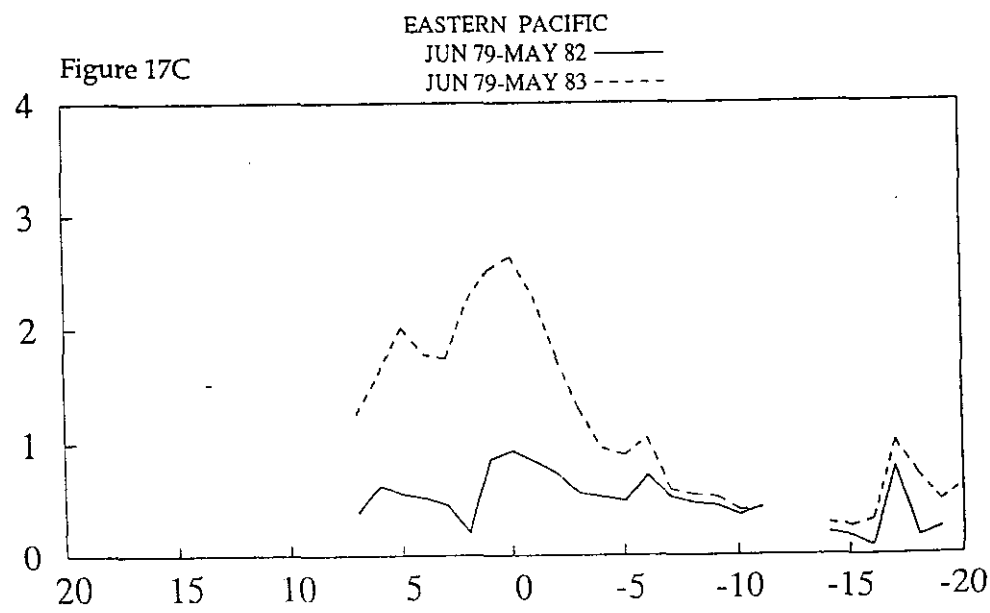

SST MERIDIONAL DECORRELATION SCALE

Figure 18A

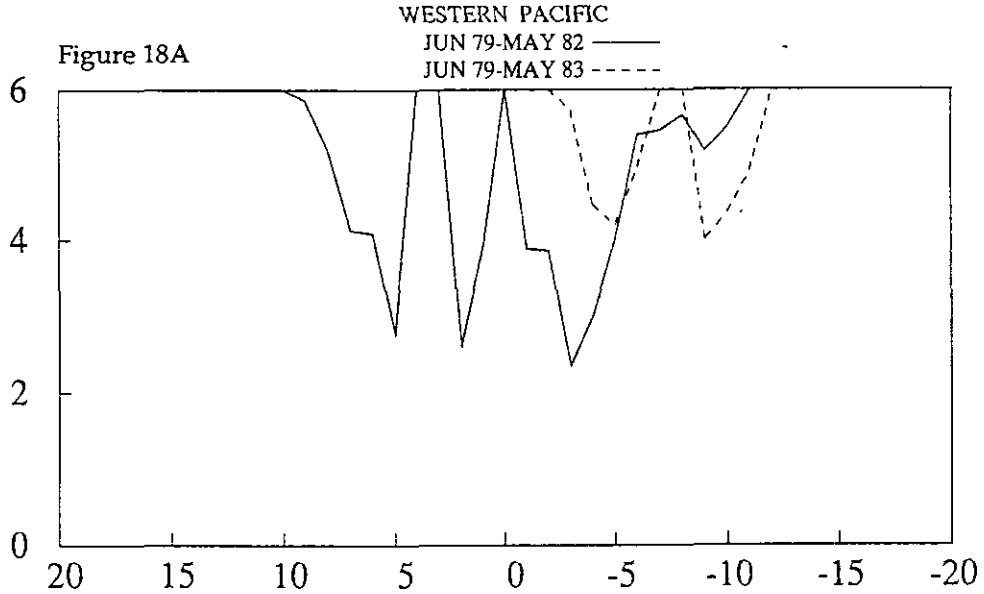

Figure 18B

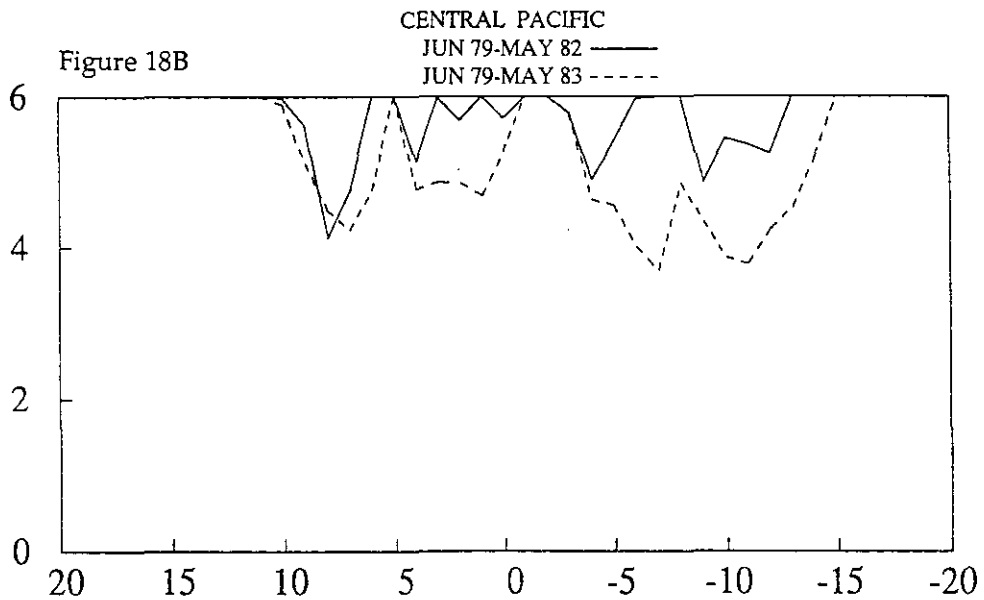

Figure 18C

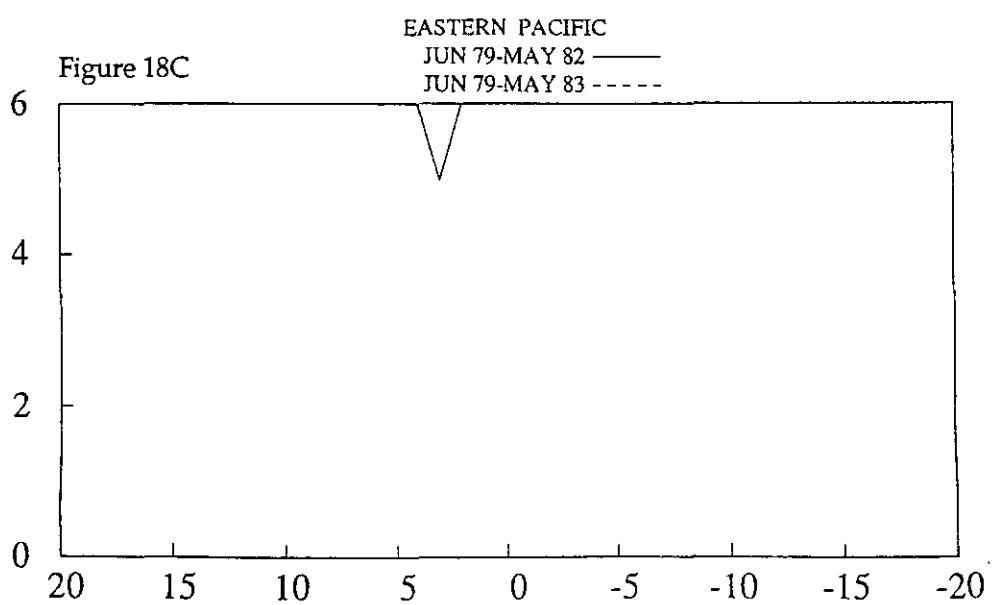

D20 MERIDIONAL DECORRELATION SCALE

Figure 19A

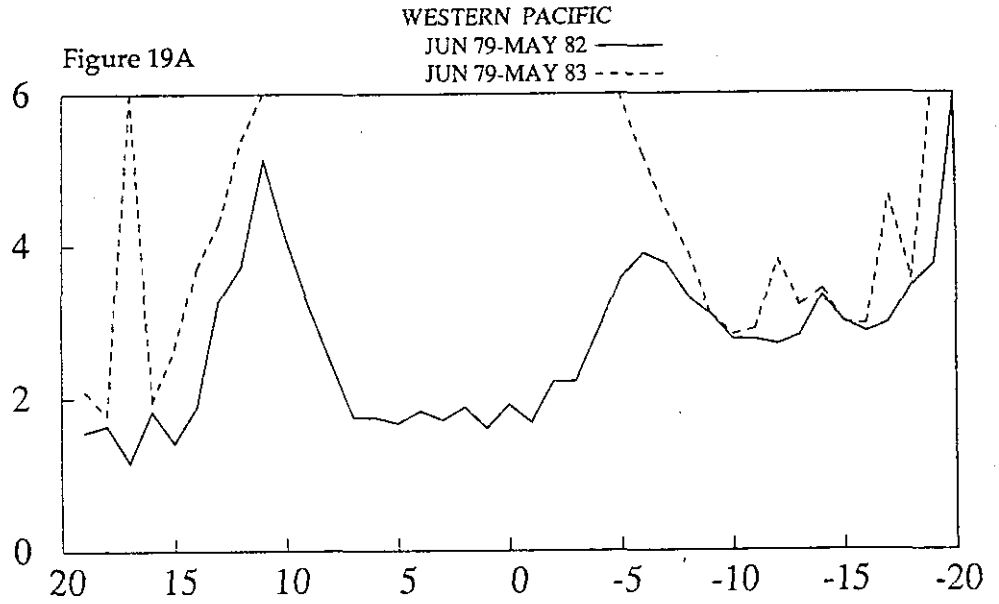

Figure 19B

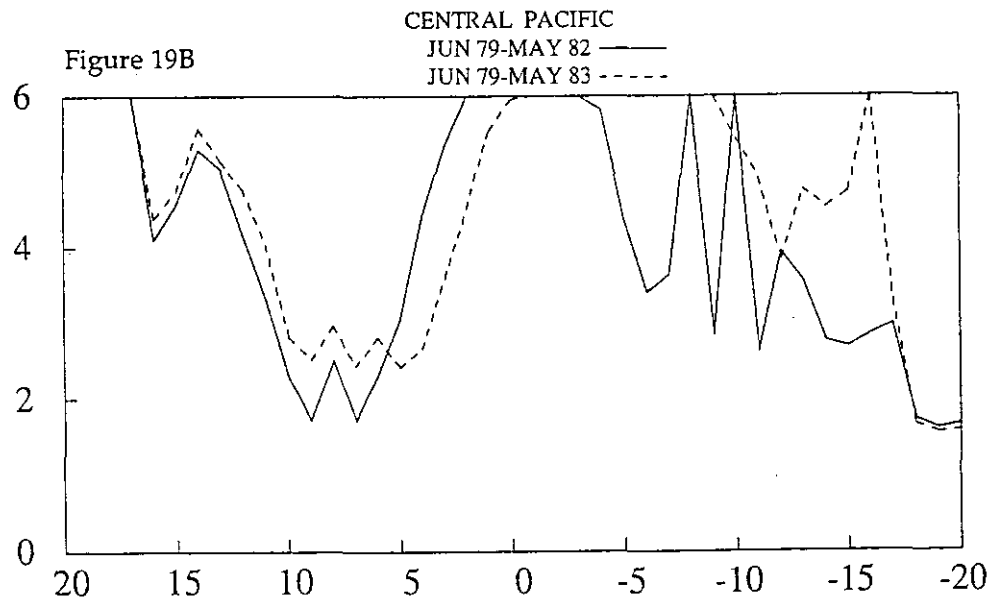

Figure 19C

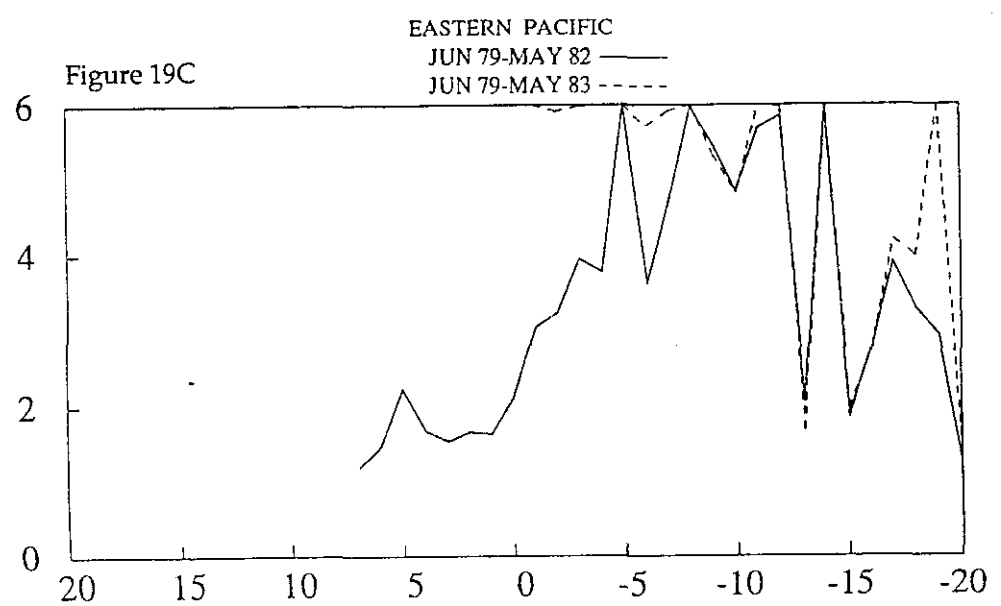

SST TEMPORAL DECORRELATION SCALE

Figure 20A

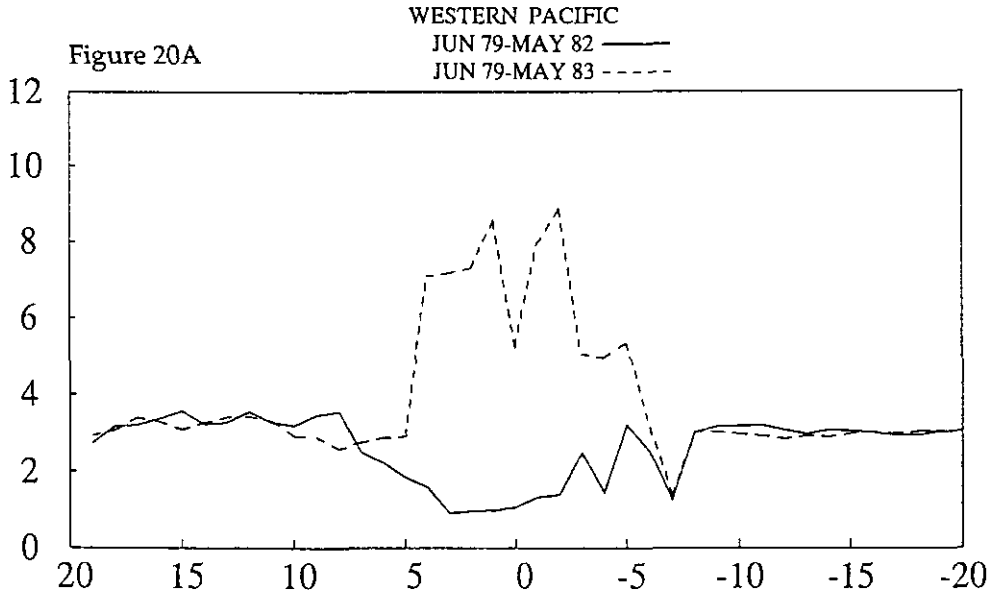

Figure 20B

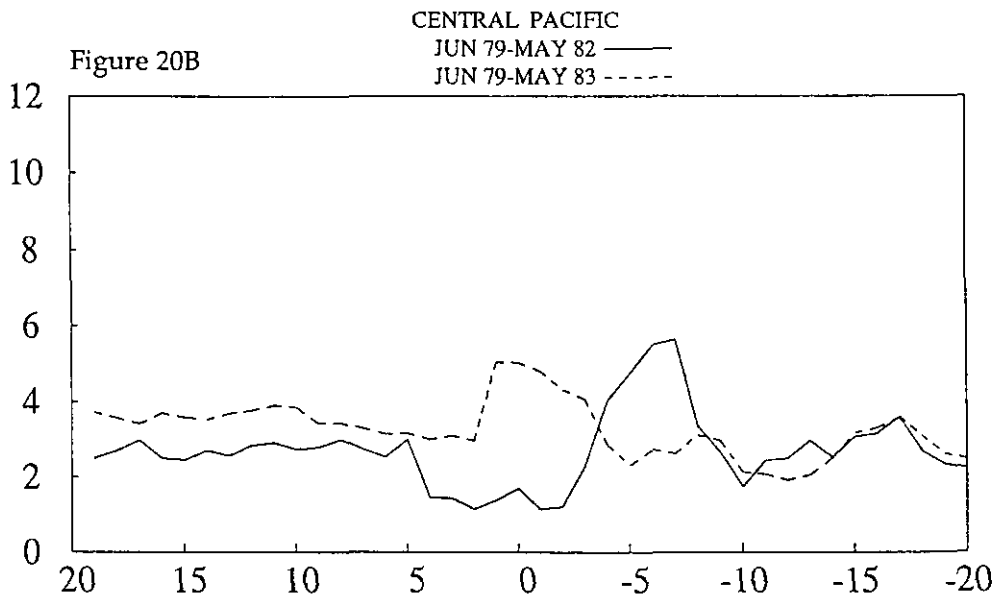

Figure 20C

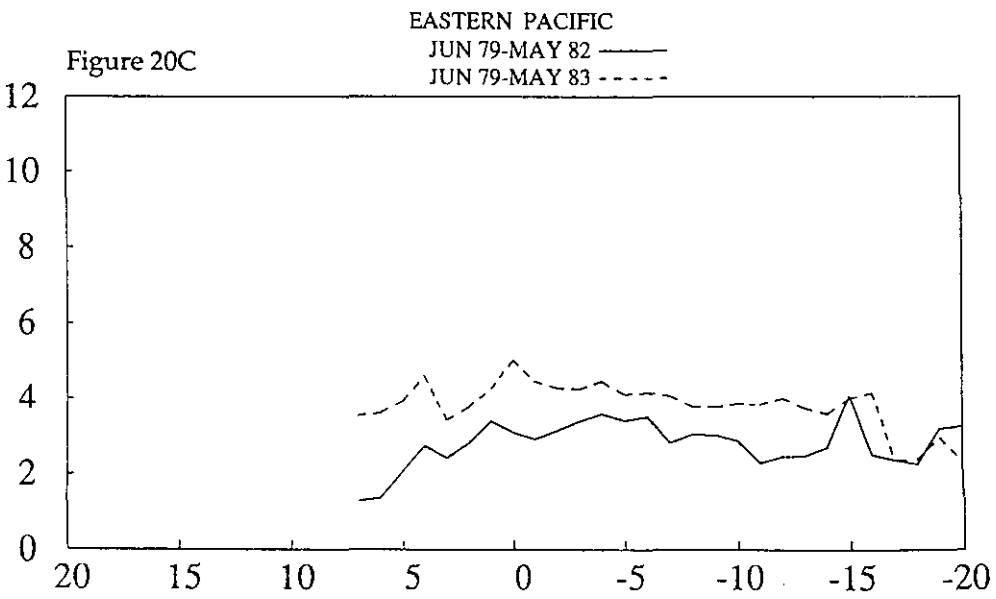

D20 TEMPORAL DECORRELATION SCALE

Figure 21A

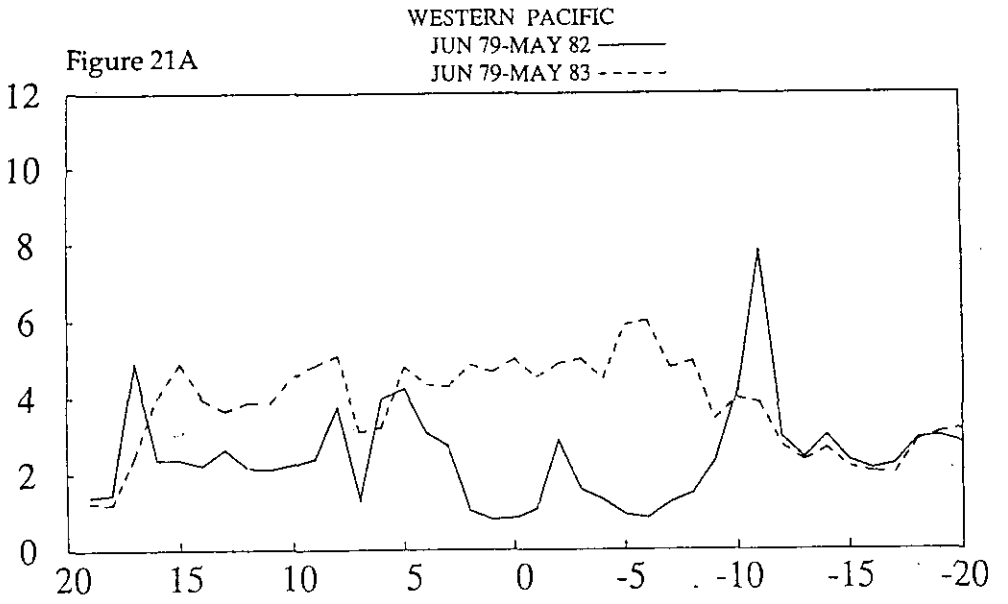

Figure 21B

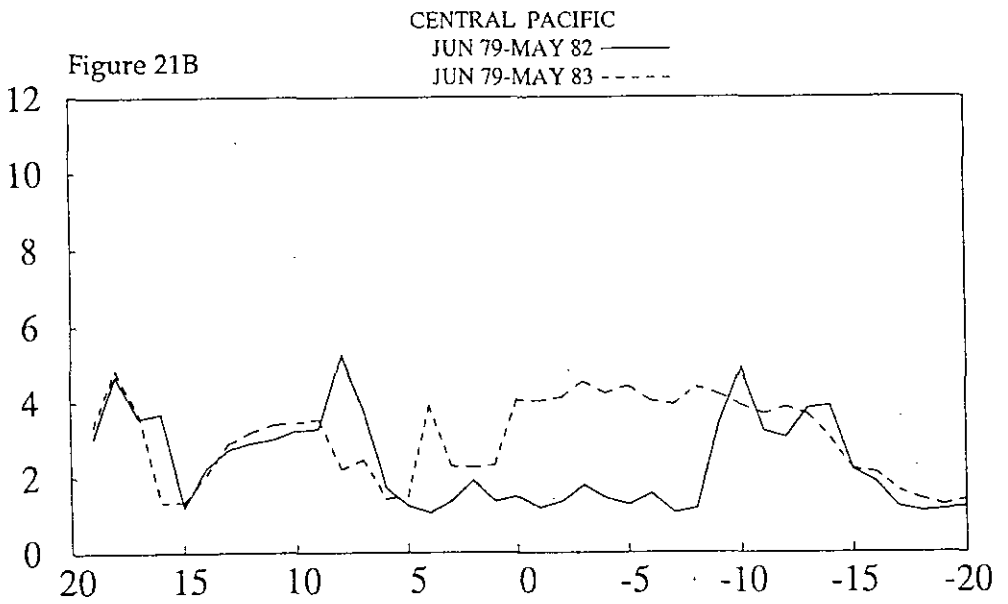

Figure 21C

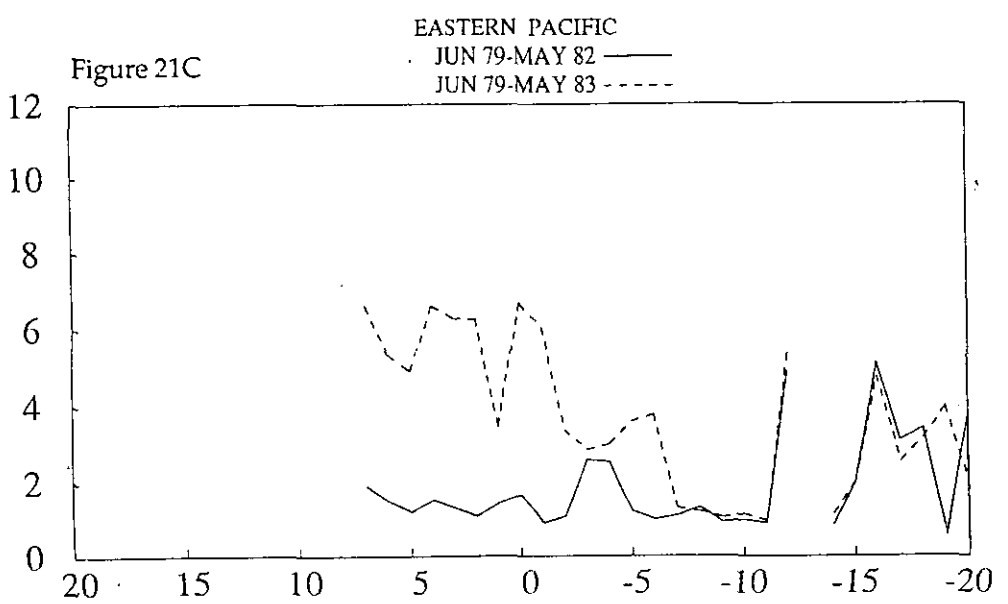

Zonal ACF Dynamic height
1949–1970

Figure 22

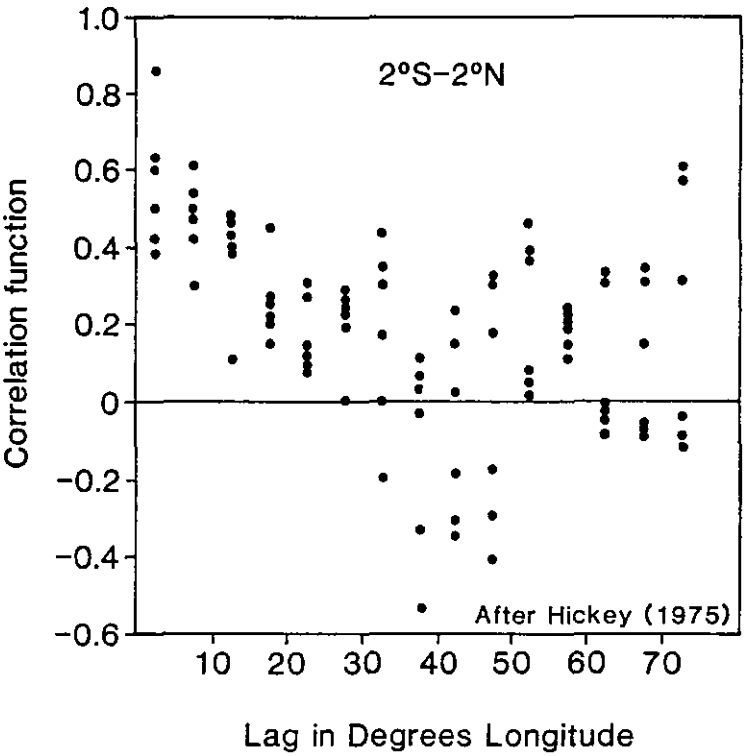

Zonal ACF Dynamic height
1946–1971

Figure 23

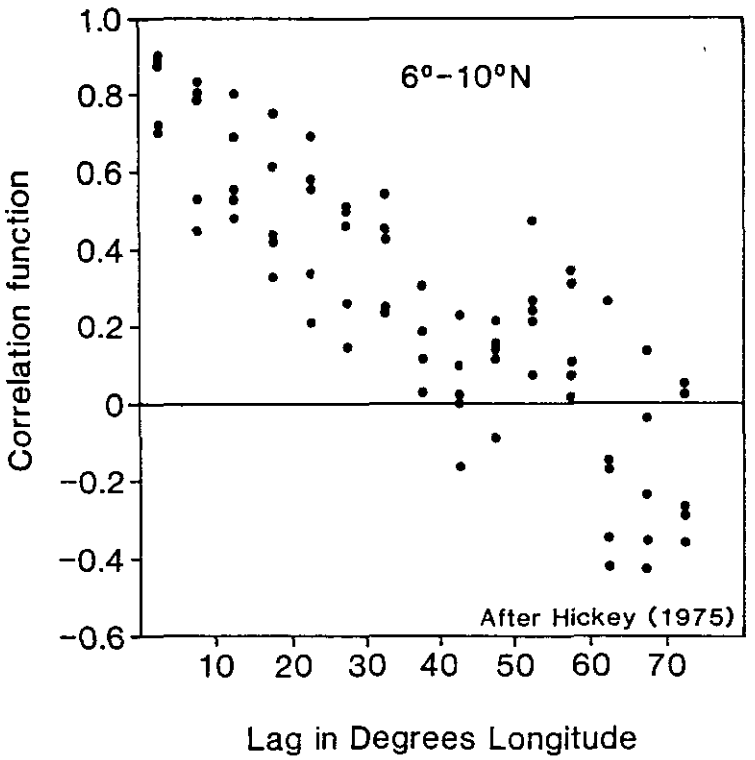

Figure 24

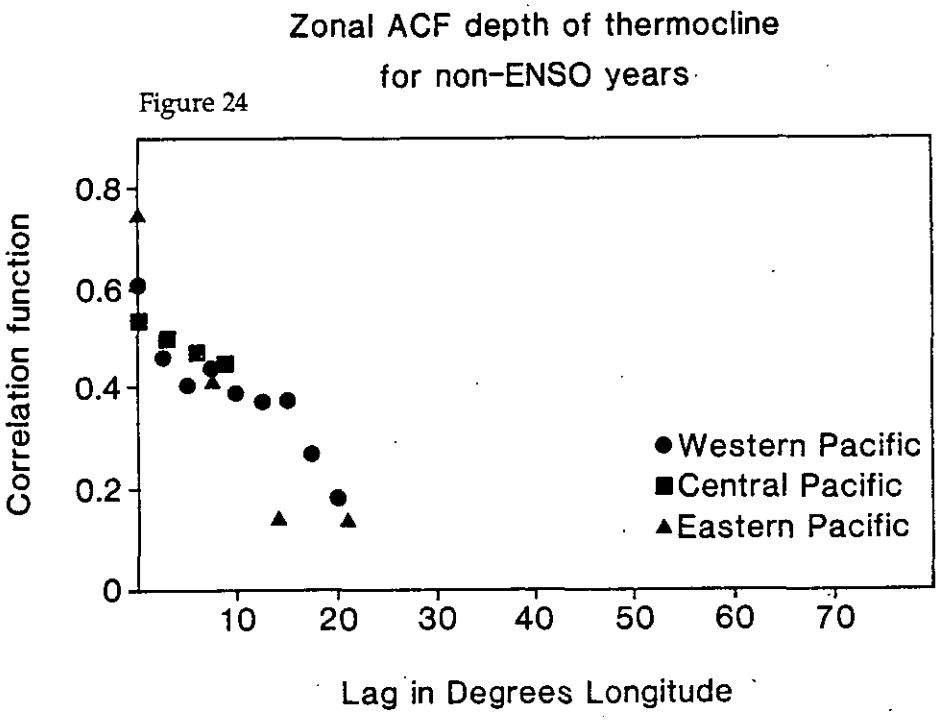

Figure 25

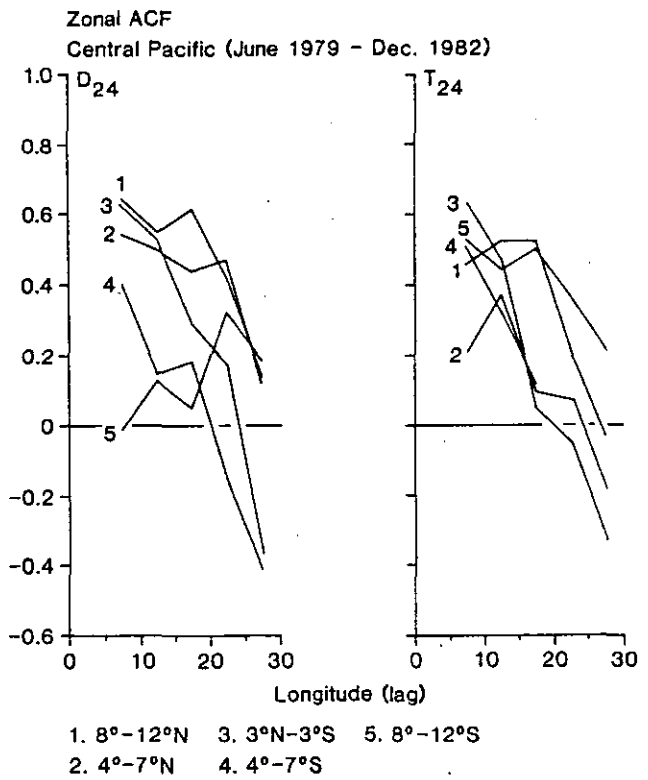

Figure 26

Pacific Ocean

Geographic Areas / Major Zonal Currents

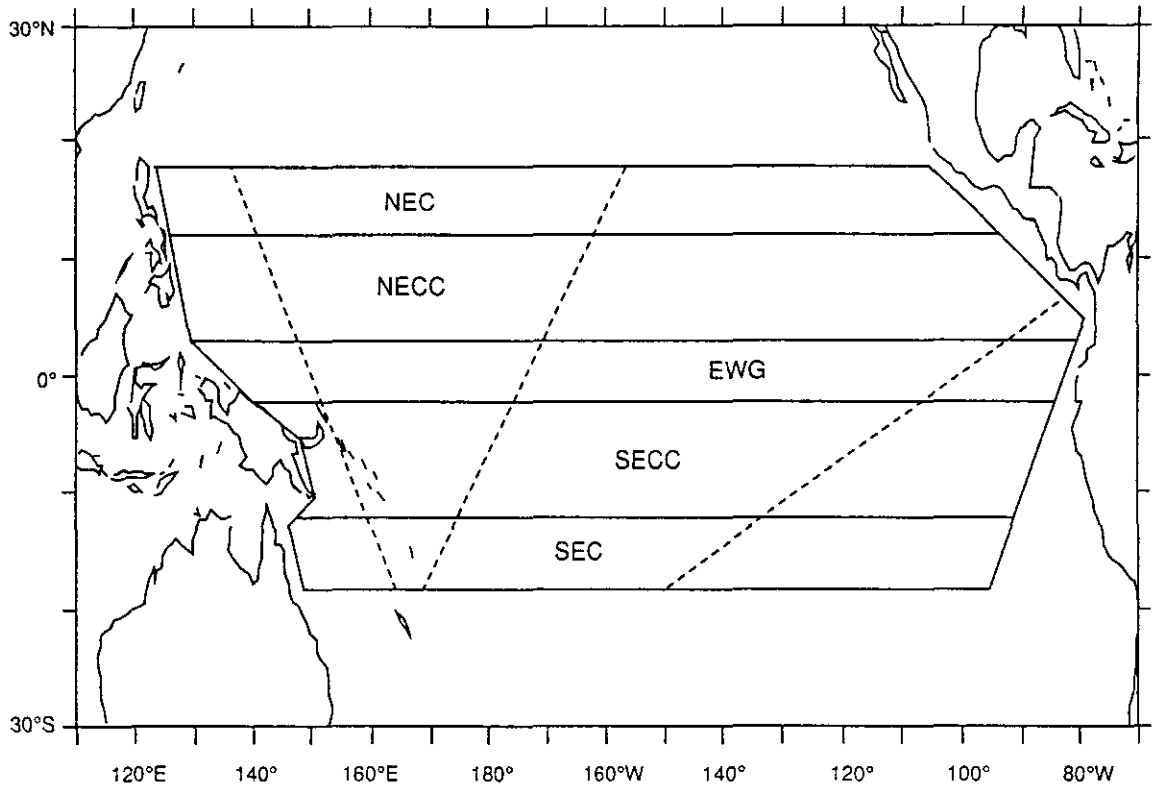

Figure 27

Signal-To-Noise Ratio / Std. Dev.

Pacific Ocean

Non-ENSO Years

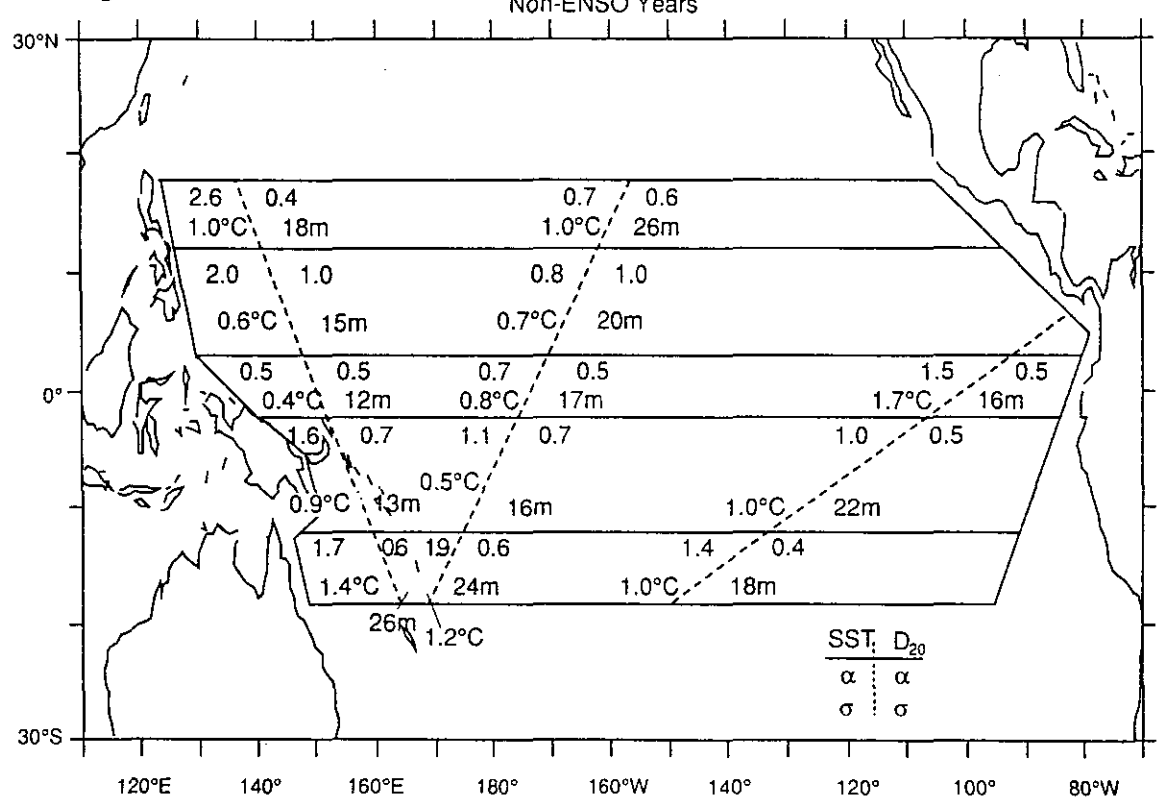

Figure 28

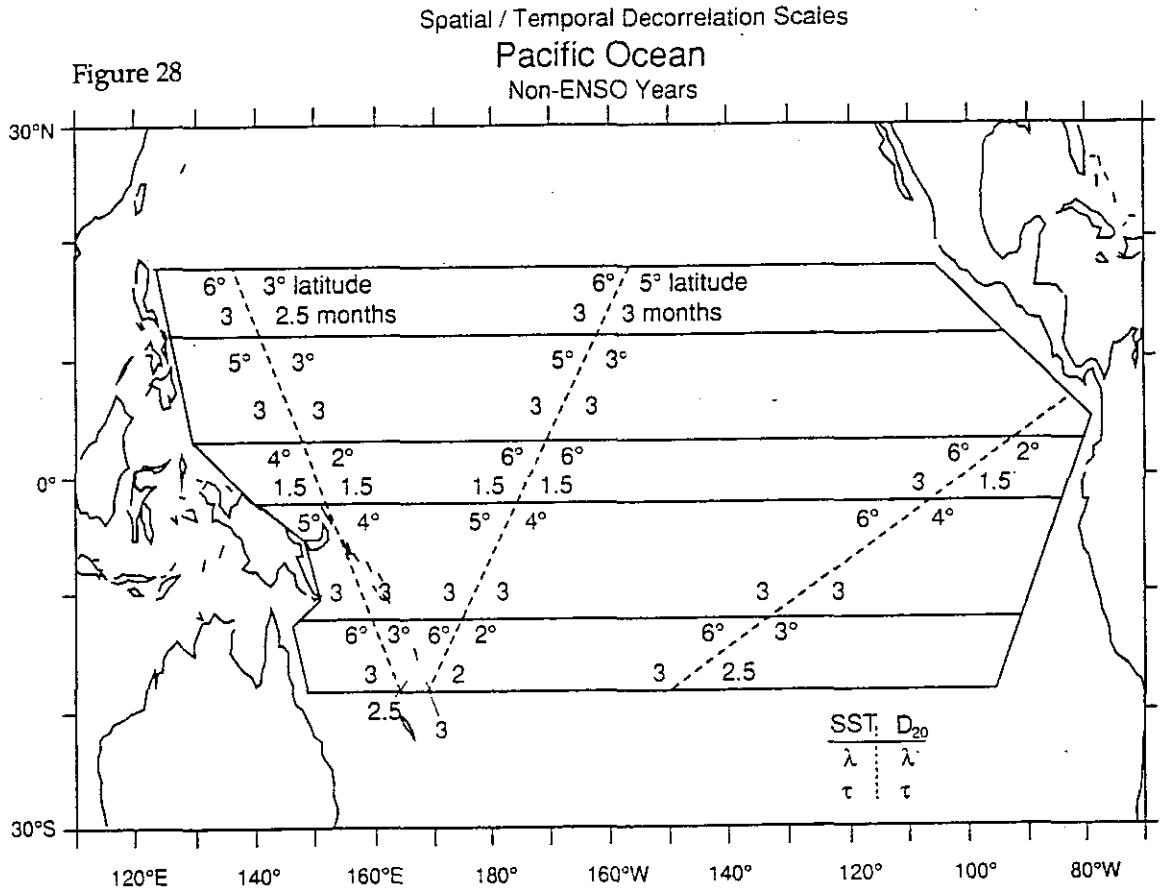
Spatial / Temporal Decorrelation Scales
Pacific Ocean
Non-ENSO Years
30°N
0°
30°S
120°E
140°
160°E
180°
160°W
140°
120°
100°
80°W
6° 3° latitude
3 2.5 months
6° 5° latitude
3 3 months
SST: D20
λ λ
τ τ

CSIRO Marine Laboratories
comprise

Division of Oceanography
Division of Fisheries

Headquarters
Castray Esplanade, Hobart, Tasmania
GPO Box 1538, Hobart, Tas 7001, Australia

Queensland Laboratory
133 Middle Street, Cleveland, Qld
PO Box 120, Cleveland, Qld 4163

Western Australian Laboratory
Leach Street, Marmion, WA
PO Box 20, North Beach, WA 6020

ISBN 0 643 04832 4.